



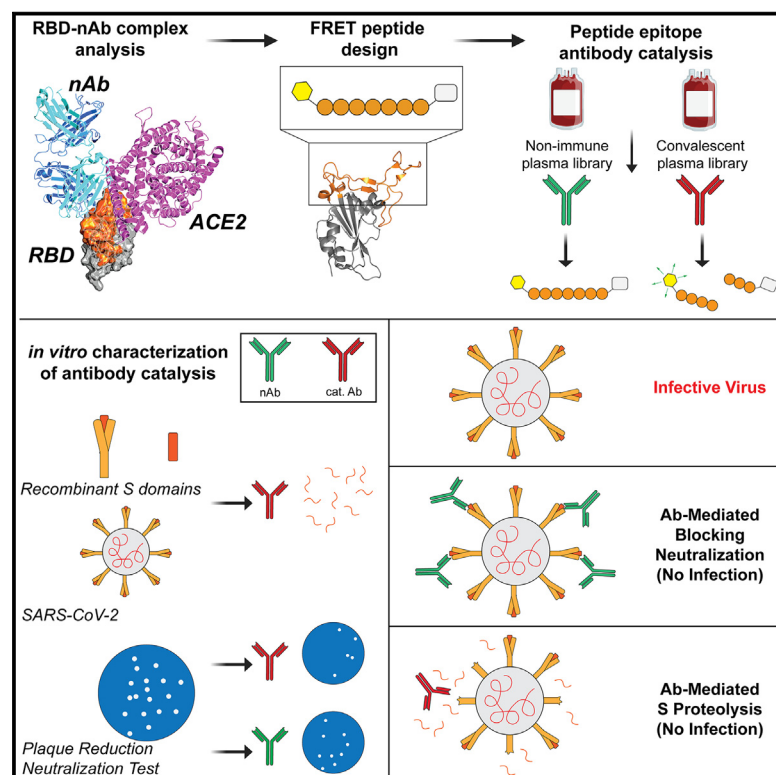
Since January 2020 Elsevier has created a COVID-19 resource centre with free information in English and Mandarin on the novel coronavirus COVID-19. The COVID-19 resource centre is hosted on Elsevier Connect, the company's public news and information website.

Elsevier hereby grants permission to make all its COVID-19-related research that is available on the COVID-19 resource centre - including this research content - immediately available in PubMed Central and other publicly funded repositories, such as the WHO COVID database with rights for unrestricted research re-use and analyses in any form or by any means with acknowledgement of the original source. These permissions are granted for free by Elsevier for as long as the COVID-19 resource centre remains active.

Cell Chemical Biology

Spike-protein proteolytic antibodies in COVID-19 convalescent plasma contribute to SARS-CoV-2 neutralization

Graphical abstract



Authors

Scott A. McConnell,
Jaiprasath Sachithanandham,
Nathan J. Mudrak, ..., David J. Sullivan,
Andrew Pekosz, Arturo Casadevall

Correspondence

acascade1@jhu.edu

In brief

McConnell et al. identify catalytic antibodies specific to the SARS-CoV-2 protein across a large panel of convalescent plasma donors. Antibody-mediated degradation of spike epitopes is correlated with viral neutralization capacity and catalysis is persistently observed despite antigenic drift of Spike in variant strains.

Highlights

- Antibodies from CCP mediate proteolysis of spike epitopes
- CCP Abs specifically proteolyze spike antigen fragments and authentic viral spike
- Spike proteolysis is a durable phenomenon despite antigenic drift in VOCs
- Antibody catalysis is a major contributing factor to viral neutralization capacity

Article

Spike-protein proteolytic antibodies in COVID-19 convalescent plasma contribute to SARS-CoV-2 neutralization

Scott A. McConnell,¹ Jaiprasath Sachithanandham,¹ Nathan J. Mudrak,¹ Xianming Zhu,⁴ Parsa Alba Farhang,¹ Radames J.B. Cordero,¹ Maggie P. Wear,¹ Janna R. Shapiro,² Han-Sol Park,¹ Sabra L. Klein,^{1,2,3} Aaron A.R. Tobian,⁴ Evan M. Bloch,⁴ David J. Sullivan,¹ Andrew Pekosz,¹ and Arturo Casadevall^{1,5,*}

¹W. Harry Feinstone Department of Molecular Microbiology and Immunology, Johns Hopkins Bloomberg School of Public Health, Baltimore, MD 21205, USA

²Department of International Health, Johns Hopkins School of Public Health, Baltimore, MD 21205, USA

³Department of Biochemistry and Molecular Biology, Johns Hopkins School of Public Health, Baltimore, MD 21205, USA

⁴Department of Pathology, Johns Hopkins School of Medicine, Baltimore, MD 21287, USA

⁵Lead contact

*Correspondence: acascade1@jhu.edu

<https://doi.org/10.1016/j.chembiol.2023.05.011>

SUMMARY

Understanding the mechanisms of antibody-mediated neutralization of SARS-CoV-2 is critical in combating the COVID-19 pandemic. Based on previous reports of antibody catalysis, we investigated the proteolysis of spike (S) by antibodies in COVID-19 convalescent plasma (CCP) and its contribution to viral neutralization. Quenched fluorescent peptides were designed based on S epitopes to sensitively detect antibody-mediated proteolysis. We observed epitope cleavage by CCP from different donors which persisted when plasma was heat-treated or when IgG was isolated from plasma. Further, purified CCP antibodies proteolyzed recombinant S domains, as well as authentic viral S. Cleavage of S variants suggests CCP antibody-mediated proteolysis is a durable phenomenon despite antigenic drift. We differentiated viral neutralization occurring via direct interference with receptor binding from that occurring by antibody-mediated proteolysis, demonstrating that antibody catalysis enhanced neutralization. These results suggest that antibody-catalyzed damage of S is an immunologically relevant function of neutralizing antibodies against SARS-CoV-2.

INTRODUCTION

Severe acute respiratory syndrome coronavirus-2 (SARS-CoV-2) is responsible for the current global pandemic of coronavirus disease-2019 (COVID-19). The genome of SARS-CoV-2 is ~79% and ~50% conserved with respect to SARS-CoV and MERS-CoV,¹ two human coronaviruses that caused serious epidemics in recent years. There is a high degree of sequence conservation in the structural and nonstructural proteins encoded by SARS-CoV-2 and SARS-CoV. One notable exception is the S protein, in which divergence is observed at key receptor-engaging residues as well as three short insertions within the N-terminal domain.² The S protein is a homotrimeric glycoprotein with two major subunits: S1 and S2. S2 comprises the highly conserved fusion machinery, while S1 mediates host receptor binding primarily through its receptor binding domain (RBD), which interacts with angiotensin-converting enzyme 2 (ACE2) receptors. The receptor binding domains in SARS-CoV-2 prefusion spike complex transiently exchange between either “open” or “closed” conformations relative to the stem of the S protein,³ where the closed conformation is incapable of receptor binding, and the open conformation is binding-competent.^{4–6}

The SARS-CoV-2 RBD has a higher binding affinity for ACE2 than the homologous receptor engaging domain in SARS-CoV,⁷ but the former predominantly assumes the closed configuration, which may aid immune evasion by partially masking neutralizing epitopes.³ Multiple proteolytic activation steps are required to loosen the sequestered RBD “closed” arrangement into the “open” conformation to allow ACE2 binding and subsequent dissociation of the S1 subunit. This in turn triggers a large rearrangement of the S2 fusion machinery that enables the insertion of the fusion peptide into the host membrane and initiation of viral fusion.^{8–10} Owing to its accessibility on the viral surface and critical function in viral fusion to host membranes, the S protein is a rational target for immunological and pharmaceutical disruption of viral pathogenesis. However, extensive glycosylation of the S protein blankets approximately 40% of the protein surface, sterically shielding many epitopes from immune recognition.¹¹ As the RBD is mostly devoid of glycosylation and houses the critical receptor binding residues, many neutralizing antibodies are directed to RBD epitopes.

Massive vaccination campaigns and monoclonal antibody therapies targeting the S protein of the ancestral SARS-CoV-2 strain initially demonstrated remarkable efficacy.^{12–16} However,

these interventions also applied significant selective pressure that yielded novel variants capable of breakthrough infections in previously immune populations.^{17,18} COVID-19 convalescent plasma (CCP) is an alternative passive antibody therapy requiring no development and low investment, and its availability is limited only by willing donors.¹⁹ Additionally, CCP provides tailored protection against specific circulating strains within a given community.²⁰ Thus, high-titer CCP has emerged as an attractive therapeutic approach, as it reduces the risk of hospitalization and decreases the risk of mortality for hospitalized patients who do not have any detectable antibodies or who are immunosuppressed.^{21–27} Because CCP contains neutralizing antibodies, the primary mechanism of CCP activity is thought to be as an antiviral agent. Higher SARS-CoV-2 neutralizing titers are associated with increased Fc-dependent functions, specifically increased complement activation, phagocytosis, and antibody-dependent cellular cytotoxicity against SARS-CoV-2-infected cells.^{28,29} Recent work suggests that antibody-mediated antigen catalysis is yet another mechanism by which CCP can neutralize virus.³⁰

Based on the transition-state stabilization theory of catalysis, the existence of antibodies with catalytic properties has long been theorized: Paratopes raised against transition-state analogs corresponding to specific chemical reactions should lower activation energy barriers for chemical conversions. In 1989, the first naturally occurring antibodies that hydrolyzed their cognate antigen were described, followed by many more examples of antibodies cleaving a diverse set of antigens.^{30–33} Although many natural catalytic antibodies have been linked to deleterious pathologies, others are associated with protective roles against microbes or in homeostasis.³¹ For example, catalytic antibodies specific to the capsule of the pathogenic fungus *Cryptococcus neoformans* have been demonstrated to cleave their antigen, resulting in altered complement deposition and increased phagocytosis.³⁰ As such, we investigated whether CCP antibodies could actively proteolyze the S protein and play a protective role in antiviral immunity. Here we report that purified antibodies from CCP catalyze the cleavage of peptide epitopes and recombinant S protein fragments, including variants of concern (VOCs) which arose after these units of CCP were collected. In addition, we show that antibody proteolysis of full-length S in the context of authentic SARS-CoV-2 virus contributes a significant portion of CCP antibody neutralization capacity, suggesting an important role for this process in viral neutralization via damage of S proteins and attenuation of receptor binding.

RESULTS

Design of peptide epitopes based on interfacial residues of RBD

The ACE2 interaction region of the S protein, known as the receptor binding module (RBM; Ser⁴³⁸-Pro⁵⁰⁷), is an extended insertion into the anti-parallel β -sheet core fold of the RBD^{34–36} (Figure S1A). The RBD-ACE2 interaction is dominated by extensive interactions with the N-terminal helix of ACE2³⁶ (Figure S1C). Antibodies with epitopes that overlap with the RBM binding site are thought to be neutralizing via competitive binding with ACE2. The complete RBM epitope is fully accessible only in the “RBD-open”

conformation, but with specific angles of approach and subepitopes, certain antibodies are capable of binding regardless of RBD conformation^{37–39} (Figures S1B and S1C). Such antibodies, belonging to the class II binding mode proposed by Finkelstein et al.,³⁸ are extremely versatile RBD binders. As such, we focused on the portion of the RBM which overlaps with the class II nAb epitope and designed two peptides intended to mimic the nAb-RBD epitope interface: RBM epitope peptide 1 (RBM1) consists of residues Lys⁴⁴⁴-Leu⁴⁵² (KVGGNYYNL) and RBM2 consists of residues Val⁴⁸³-Ser⁴⁹⁴ (VEGFNCYFPLQS) (Figures 1B and S1C). The biological interface between RBD and ACE2 encompasses 864 Å² of surface area, of which RBM1 and RBM2 contribute 10% and 39% of the total interface, respectively. Of the five critical residues for ACE2 engagement, RBM2 contains three (F486, Q493, and S494) and RBM1 has none.¹ With respect to the immunological interface formed with a representative class II neutralizing antibody P2B-2F6, RBM1, and RBM2 encompass interfaces of 329 and 327 Å², respectively, which together account for the complete interface (Figure S1C). Thus, cleavage of the RBM2 sequence would likely result in direct disruption of ACE2 recognizing residues, while cleavage of the more readily accessible RBM1 site could exert indirect structural changes that may interfere with ACE2 engagement.

High-throughput assay to detect RBM peptide epitope proteolytic cleavage

These two RBM epitopes were synthesized as quenched fluorescent peptides to generate sensitive fluorescent resonance energy transfer (FRET) reporters of RBM-specific proteolysis. Each RBM peptide was appended with an Mca fluorophore and Dnp quencher at its N- and C-termini, respectively (Figure 1A). In a pilot screen to assess the catalytic cleavage of RBM-derived peptides by convalescent antibodies, we selected four random aliquots of CCP units obtained near the onset of the pandemic (June 2020). These CCP units varied markedly in specific antibody titers (~5 ng/mL–5 μ g/mL, Table S1), which was expected given that neutralizing titers are highly variable among individuals who have recovered from COVID-19.⁴⁰ Each CCP unit was incubated with a single quenched fluorescent peptide under physiological conditions (37°C) for 5 h. Fluorescence was monitored over time and converted to molarity of substrate using the maximal fluorescence observed in proteinase K control reactions, which represent complete proteolysis of each peptide. RBM cleavage was observed for every CCP sample in our pilot study, although cleavage velocities varied (Figures 1C and S2, and Table S1). Further, catalytic activity did not increase in a dose-dependent manner, but instead diminished at higher concentrations of convalescent plasma (Figures S2 and S3, and Table S1). Such impairment of immune complex formation at exceedingly high antibody concentrations, which results in lower activity for concentrated samples above a critical threshold, is known as the hook or prozone effect.^{41–43} Observation of this phenomenon in our kinetics data strongly suggests an antibody-mediated competition phenomenon.

Next, we sought to confirm that the observed cleavage was antibody-mediated, rather than from spurious cleavage from canonical proteases or other catalytic components found in human plasma. Non-immunoglobulin components in CCP were denatured by heat treatment at 55°C, a temperature routinely

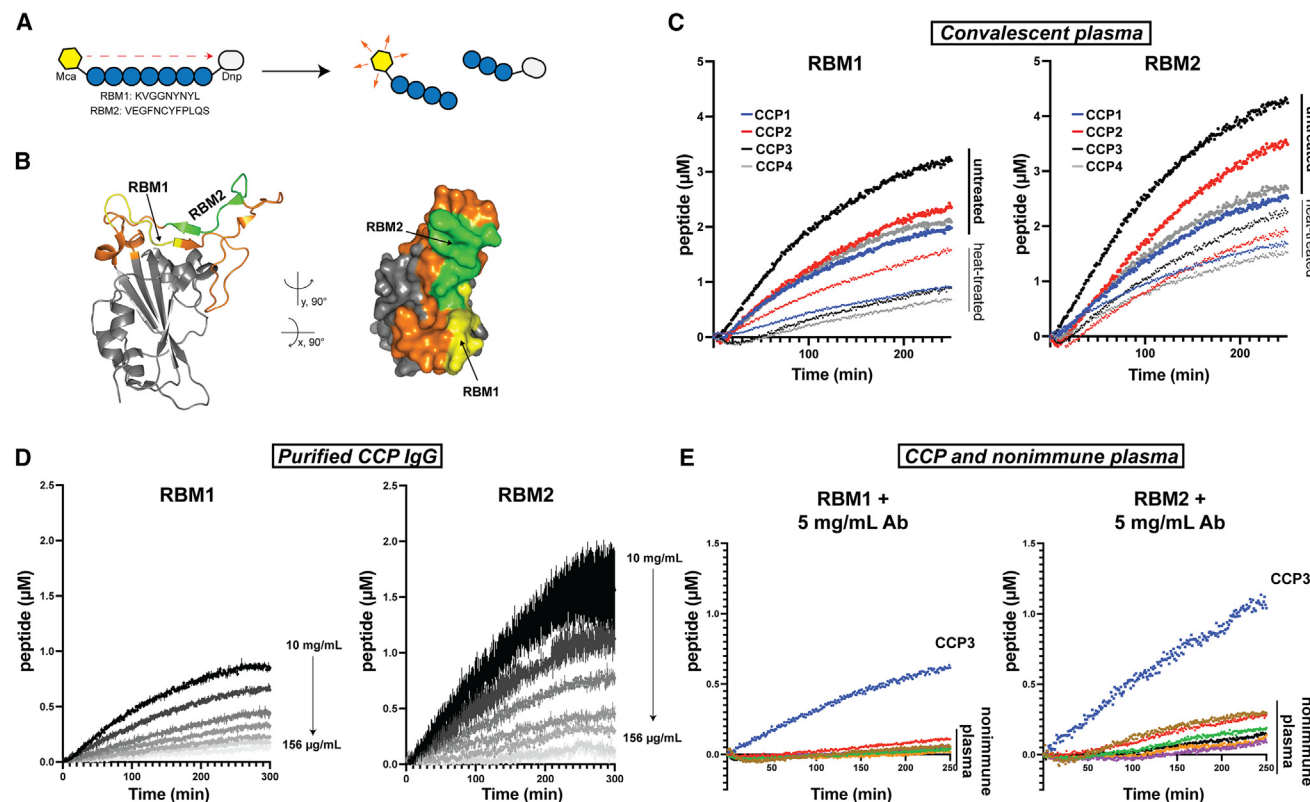


Figure 1. Antibody-mediated antigen FRET proteolysis assay with purified IgG from CP donors

(A) Schematic of FRET proteolysis principle employed in this assay. Mca fluorophore and Dnp quencher pairs were appended to the N- and C-termini of each RBM epitope peptide. Intact peptides do not fluoresce when excited by a 320 nm laser line due to resonance energy quenching by the covalently attached Dnp quencher. When the intervening peptide backbone is cleaved, quenching is relieved and fluorescence is observed.

(B) The locations of the two FRET peptide sequences on the tertiary structure of the receptor binding domain are highlighted (RBM1, yellow; RBM2, green).

(C) FRET kinetic traces illustrate the relative activity of untreated and heat-treated convalescent plasma from four different donors (labeled CCP1-4, 2-fold dilution of CCP). See Figure S2 and Table S1 for full CCP kinetic data.

(D) The concentration of purified CCP3 antibodies was titrated from total antibody concentrations of 10 mg/mL to 156 μ g/mL to measure the dose dependence of antibody concentration on peptide cleavage. See Table S2 for full kinetic CCP IgG kinetic data. Each kinetic curve is displayed as the mean \pm S.D. of 2 replicates, and fluorescence measurements were converted to units of molarity of proteolyzed peptide epitope using each corresponding positive control.

(E) The kinetic traces of peptide proteolysis mediated by CCP3 and a set of six nonimmune plasma samples are overlaid, where 5 mg/mL of purified total IgG from each plasma sample was incubated with RBM FRET epitopes. Cleavage of RBM1 and RBM2 epitopes are displayed on the left and right, respectively. See Figure S5 and Table S3 for full nonimmune IgG kinetic data.

used to inactivate complement proteases while sparing highly thermostable antibodies.^{44,45} A comparison of the activities from heat-treated versus untreated plasma samples demonstrated that 40–55% of activity was retained after heat treatment (Figure S2 and Table S1). The attenuation of observed proteolysis may also be due to the reduction in specific antibody catalysts, as 2-fold reductions of IgG and IgM titers were observed following similar heat-inactivation procedures.⁴⁶ Proteolysis rates of RBM2 across the four CCP units tested here were, on average, 32% faster than for RBM1 for untreated plasma, and 86% faster than RBM1 cleavage rates by heat-treated plasma. CCP3 has a relatively high proportion of RBD-specific IgG and exhibited up to 40% faster initial velocities of RBM proteolysis than the other CCP tested (Table S1). Interestingly, the proportion of RBD-specific antibody did not directly determine catalytic activity in the heat-treated CCP samples characterized here, as CCP containing lower levels of RBD-specific antibody demonstrated comparable cleavage

activity to higher specific titer plasma (Figure S3). Heat-inactivated nonimmune plasma obtained from a donor never exposed to SARS-CoV-2 proteolyzed RBM1 and RBM2 at velocities 97% and 34% of that observed for CCP3 (Figure S4). RBD-specific antibody was depleted from CCP3 using RBD-conjugated magnetic beads, resulting in a 2.2-fold reduction of RBD-specific immunoglobulin (Figure 2A). Peptide cleavage by α -RBD Ab-depleted CCP3 relative to untreated CCP3 was attenuated by 6% and 27% for RBM1 and RBM2, respectively (Figures 2B and 2C). Thus, RBD-specific antibody has an outsized contribution to overall catalysis given that it comprised only 0.04% of the total IgG in CCP3.

Next, to evaluate immunoglobulin-mediated catalysis separately from any proteolytic contributions from non-antibody components in plasma, we purified IgG from CCP3, which had the highest RBD-specific antibody titers and fastest RBM2 cleavage velocity after heat treatment. We subjected this affinity-purified polyclonal CCP3 IgG to the same FRET

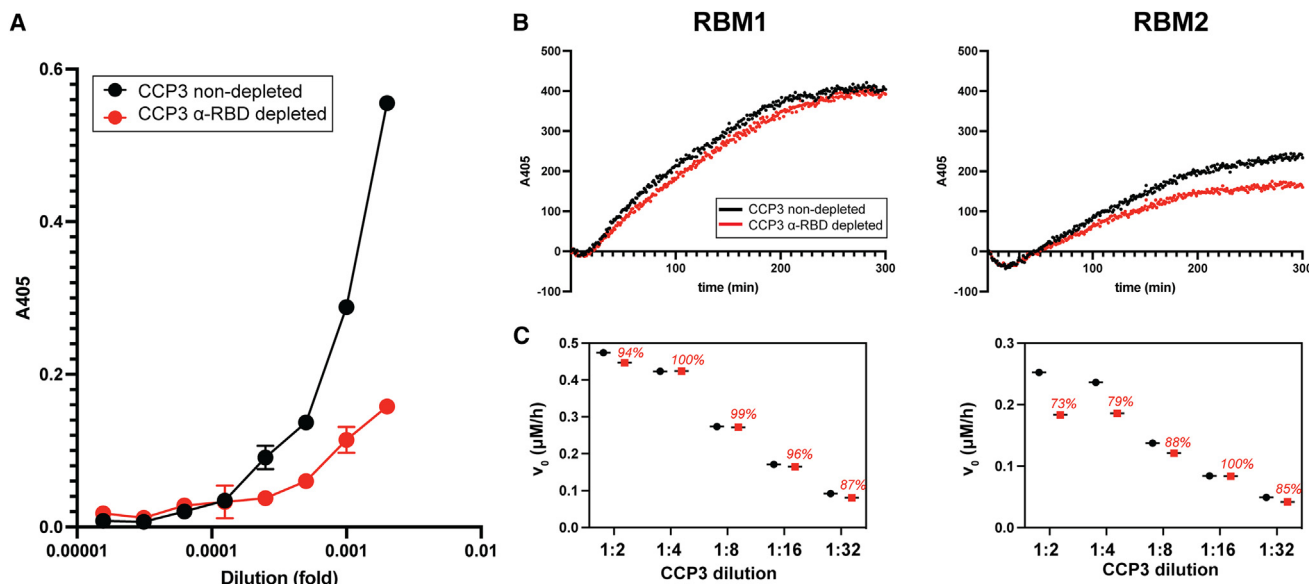


Figure 2. RBD-specific antibody depletion of CCP3 by adsorption to magnetic beads results in attenuation of cleavage activity

(A) Depletion of RBD-specific antibody from heat-treated CCP3 using RBD-conjugated magnetic beads was confirmed by quantitative ELISA. Absorbance values at 405 nm for untreated (black) or bead-depleted CCP3 (red) are graphed as the mean \pm S.D. of 2 replicates for each successive serial dilution and calculated RBD-specific IgG concentrations are indicated.

(B) FRET kinetics of heat-treated CCP3 compared to heated-treated CCP3 depleted of RBD-specific antibody with RBD-conjugated magnetic beads. Fluorescence values for non-depleted CCP3 (black) and bead-depleted CCP3 (red) are displayed for the 2-fold dilution. Each sample was measured in duplicate.

(C) Calculated initial velocities for depleted and non-depleted CCP3 at each serial dilution tested are displayed, with the percent initial velocity of RBD-depleted CCP3 with respect to the corresponding dilution of non-depleted CCP3 are indicated with red labels.

screen using a total IgG concentration in the range of 156–10,000 $\mu\text{g/mL}$ (0.04–2.78 $\mu\text{g/mL}$ α -RBD IgG). We observed significant catalytic activity in the purified antibody sample, which increased in a dose-dependent manner, as total antibody concentrations were kept below the prozone threshold (Figure 1D and Table S2). Affinity-purified IgG from six nonimmune plasma donors was also characterized to establish a baseline of the cross-reactive cleavage of nonimmune IgG. We measured initial proteolytic velocities for RBM1 and RBM2 in the ranges of 0.0005–0.024 $\mu\text{M/h}$ and 0.002–0.078 $\mu\text{M/h}$, respectively (Figures 1E and S5, and Table S3). Compared to the initial velocities observed by antibody isolated from CCP3 at the same total antibody concentration (0.165 and 0.255 $\mu\text{M/h}$ for RBM1 and RBM2), this represents 0–15% and 1–30% of the observed velocity by CCP3 for each epitope. Importantly, we noted that the relationship between the concentration of α -RBD IgG and peptide cleavage velocity observed for the affinity-purified CCP3 IgG was comparable to that of heat-treated total CCP3, indicating that heat treatment effectively separates nonspecific cleavage by serum proteases from antibody-mediated cleavage and can be used as a proxy for cleavage by pure IgG in larger screens where individual purification is impractical (Figure S3).

RBM proteolysis correlates with CCP neutralization and other attributes

After establishing a robust high-throughput FRET assay for RBM epitope cleavage, we deployed our FRET proteolysis assay on two collections of diverse CCP samples to ascertain if anti-

body-mediated cleavage efficiency corresponded to relevant immunological characteristics. In the first library, heat-treated CCP from 46 random donors was screened for proteolytic cleavage of the RBM peptides. Significant inverse relationships were observed for cleavage of both RBM peptides and patient age ($R = -0.387$, $p = 0.008$ and $R = -0.719$, $p < 0.001$ for RBM1 and RBM2, respectively), and the negative correlation of peptide cleavage to time since diagnosis closely approached the significance threshold ($R = -0.282$, $p = 0.057$ and $R = -0.281$, $p = 0.059$) (Figure S6A). However, there was no significant correlation between S1-specific antibody titers measured by EuroImmuno and RBM cleavage (Figure S6A). We then screened a second library of 126 CCP samples⁴⁰ to investigate the relationship between antibody-neutralizing function and cleavage activity. We observed a weak positive correlation between total RBM1 cleavage and microneutralization assay area under the curve (AUC) values ($R = 0.178$, $p = 0.047$), indicating that antibody-mediated cleavage may contribute to the neutralization of SARS-CoV-2 (Figure S6B). We also found a correlation between RBD-specific antibody titers and the RBM1 cleavage, supporting the notion that cleavage is associated with a specific antibody.

Antibody-mediated epitope cleavage is catalyzed through several mechanisms

To gain a better understanding of the types of proteolytic mechanisms employed by catalytic antibodies in the in polyclonal mixture, we subjected affinity purified antibody from CCP3 to a protease inhibitor screen. We assessed the relative inhibition of five specific protease inhibitors to gain insight into the

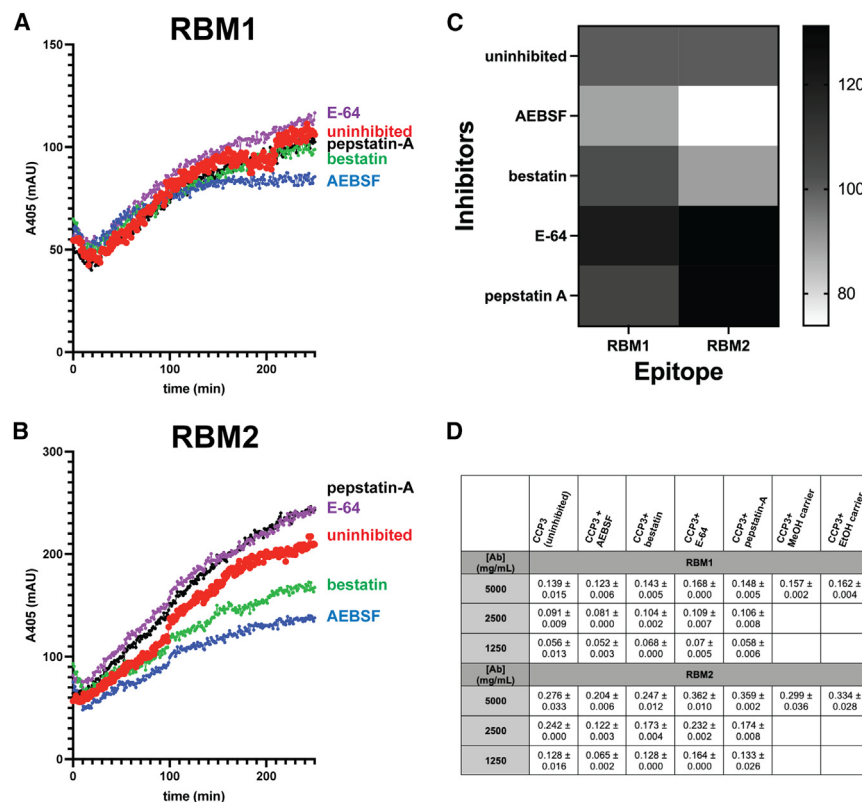


Figure 3. Protease inhibitor screens yields mechanistic insights in antibody catalytic mechanism

(A and B) RBM epitope probes were incubated with CCP3 IgG in the presence of a set of protease inhibitors to gain insight into the mechanism of action. Kinetic traces of the reaction in the presence of AEBSF, bestatin, E-64, pepstatin-A, and without inhibitor are displayed in blue, green, purple, black, and red, respectively. Panel A and B show the mean cleavage of two replicates at 5 mg/mL CCP3 IgG for RBM1 and RBM2 peptide probes, respectively.

(C) A heatmap of the initial velocities of each reaction + inhibitor at 5 mg/mL, normalized to the corresponding uninhibited velocity.

(D) Full table of initial velocities of cleavage for CCP3 in presence of each inhibitor at all antibody concentrations.

contribution of each mechanism of action in the catalytic antibody population: AEBSF (serine proteases), bestatin (aminopeptidases), E-64 (cysteine proteases), and pepstatin-A (aspartic acid proteases). We did not observe any appreciable inhibition by E-64 or pepstatin-A, but measured a 42% and 13% inhibition of RBM2 cleavage was observed for AEBSF and bestatin, respectively, indicating that a fraction of antibodies in the convalescent antibody population utilize serine protease and aminopeptidase-like mechanisms (Figure 3).

CCP antibodies cleave authentic S protein and recombinant fragments

After determining that convalescent antibodies cleave RBD peptide epitopes and that this activity was associated with virus neutralization across a large CCP library, we investigated whether the catalytic antibodies could also cleave full S proteins in more stably folded tertiary configurations. Incubation of purified CCP3 antibodies with recombinant RBD (rRBD) or S1 (rS1) protein domains for 7 days resulted in clear proteolytic degradation of the full-length protein (Figures 4A and 4B). The residual band intensity of intact rRBD decreased in a dose-dependent manner with respect to rRBD incubated at 37°C in the absence of antibody. Incubation with CCP3 antibody in the range 250–2000 µg/mL total IgG (70–560 ng/mL α-RBD IgG) resulted in 20–78% degradation of rRBD. Under the same conditions, rS1 protein was degraded 21–59%. Under these reaction conditions, purified CCP3 antibody demonstrated a range of cleavage rates from 0.45–1.75 nM/h and 0.82–2.30 nM/h when rRBD or rS1 were used as substrates, respectively. Further, we confirmed that the proteolysis observed in these assays was specific to S

proteins, as no detectable degradation was observed when we incubated an irrelevant protein, bovine serum albumin, in similar reaction conditions with purified antibodies from three different CCP units (Figure S7). To confirm that the observed activity extended to full-length S protein on authentic SARS-CoV-2 virus particles, we examined the effect of CCP3 IgG incubation with inactivated SARS-CoV-2 virus

(Figure 4C). Although the degree of degradation was less than observed for recombinant S proteins in similar conditions (0–15% band reduction compared to no-antibody control), we also observed the concomitant accumulation of degradative S fragments.

Antibody proteolysis enhances virus neutralization

Given that CCP antibody proteolyzes S protein on authentic SARS-CoV-2, we next sought to directly measure the impact of antibody catalysis on the ability of the virus to infect human cells. As traditional human enzymes have optimal activity at physiological temperature, we reasoned that lowering the temperature could substantially reduce catalysis by antibodies. Indeed, antibody-mediated cleavage of rRBD was significantly attenuated below physiological temperatures (<37°C), and nearly undetectable at 4°C (Figures 5A and 5B). Thus, we designed a plaque reduction neutralization test (PRNT) protocol that involved differential temperature preincubations of antibody with virus to separate antibody binding of epitopes from antibody-mediated epitope proteolysis (i.e., incubation with virus at physiological temperature activates antibody-mediated proteolysis, while incubation at 4°C allows binding but inhibits proteolysis). The incubation period of virus and antibody was also extended from the 1 h incubation used in standard viral neutralization assays to 6 h to allow sufficient proteolysis to occur. Given that antibody-antigen binding is an enthalpically driven reaction, we hypothesized that binding should be more favorable at a low temperature given the lessening effect of the temperature-weighted entropy term. This was confirmed by indirect ELISA where the antibody was bound to RBD antigen under

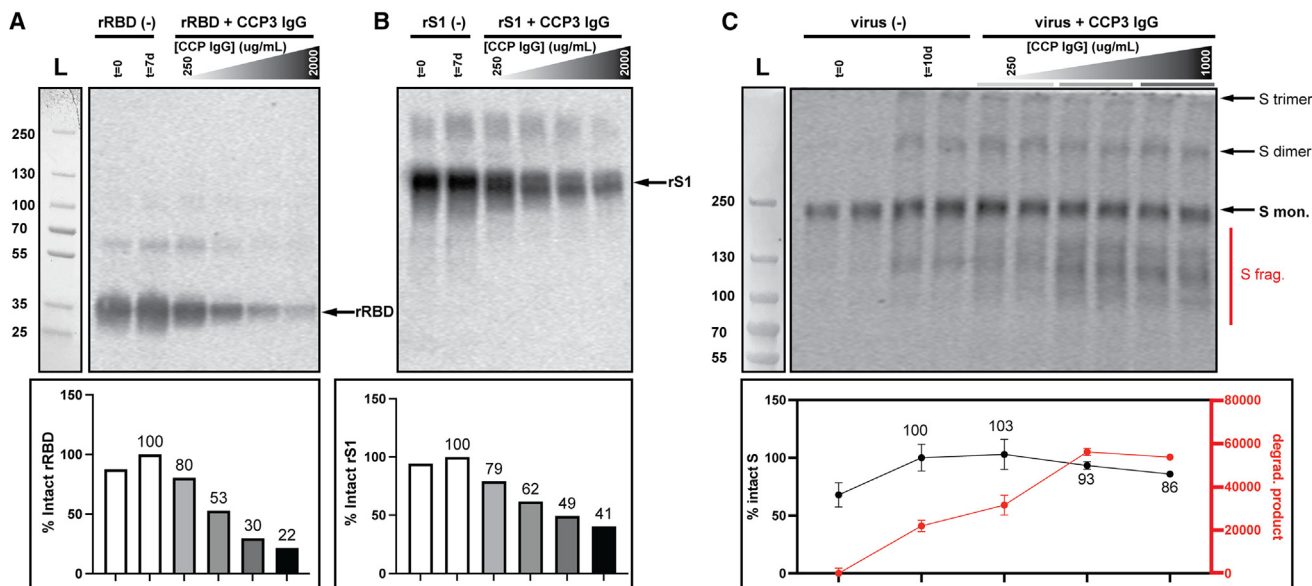


Figure 4. Recombinant RBD and S1 is degraded by purified antibody from CCP3

Digestion reactions of recombinant S protein fragments were separated by SDS-PAGE and probed for residual S protein by immunoblot. The relative amount of intact S protein remaining after each digestion reaction was quantified by normalizing band intensity of rRBD or rS1 or authentic viral S in the no-antibody control to each experimental reaction.

(A) Recombinant RBD (10 μg/mL) was incubated with 250–2000 μg/mL purified IgG from CCP3 for a period of 7 days.

(B) Recombinant S1 (50 μg/mL) was incubated with 250–2000 μg/mL purified IgG from CCP3 for a period of 7 days.

(C) Inactivated SARS-CoV-2 virus (50 μg/mL) was incubated with 250–1000 μg/mL CCP3 antibody for a period of 10 days. Each reaction was run in duplicate and the location of S protein monomer, multimers and proteolytic fragments is indicated. Below each panel (A–C), the relative amount of intact S remaining in each digestion reaction with a gradient of purified IgG from CP was quantified by normalizing band intensity of S in the no-antibody control the same incubation. In panel C the relative band intensity of proteolytic degradation species (defined as cumulative band intensity below the S protein monomer) was quantified and noise-corrected by subtracting intensity measured in the same search area for the no-antibody control for full virus incubations. Molecular weight ladders from the aligned Coomassie-stained gels are shown for reference and labeled with L. The molecular weight marker in panel A refers also to panel B, as both experiments were on the same gel.

the same conditions as in the modified PRNT, revealing that binding was roughly equivalent at the two temperatures (Figure 5C). Therefore, antibody-viral complexes should form with equal affinity at the two different temperatures used in this assay and differences in neutralization activity reflect only the contribution of antibody-mediated catalysis.

Modified PRNT assays were performed at three different temperatures using heat-treated CCP3 with SARS-CoV-2 A.3 isolate HP00076. Samples incubated at 37°C achieved a geometric mean IC_{50} of 619.8 (95% CI 404.9, 948.8), while the 4°C and room temperature (RT) were found to be 137.5 (95% CI 93.75, 201.8) and 118 (95% CI 54.75, 254.1), respectively (Figures 6A and 6B). The 4°C and RT showed statistically significant lower geometric mean IC_{50} values compared to 37°C, with the fold difference ranging from 1.16- to 5.25-fold. Next, purified IgG from CCP3 was tested in the same live virus neutralization assay. The geometric mean for the samples incubated at 37°C was IC_{50} of 770 μg/mL (inverse IgG dilutions; 95% CI 274.8, 2157), followed by 208.4 μg/mL (95% CI 131.9, 329.2) and 259.5 μg/mL (95% CI 253.2, 265.9; Figure 6C) for RT and 4°C. The 4°C and RT showed statistically significant lower geometric mean IC_{50} values than 37°C, with the fold difference ranging from 1.25- to 3.69-fold. The finding that the fold-increase observed for heat-treated CCP3, containing the full complement of antibody subtypes, was greater than purified

polyclonal IgG suggests that antibodies of other isotypes are similarly catalytically active.

Variant S proteins are still susceptible to proteolysis by CCP obtained prior to variant emergence

Given that the four main CCP samples analyzed in this study were acquired near the beginning of the pandemic when the ancestral SARS-CoV-2 strain predominated, we were interested in whether substitutions found in the S protein from subsequent VOC (VOC) affected antibody-mediated proteolysis. Mutations frequently associated with VOC within the RBM epitopes used in this study (residues K444-L452 and V483-S494) were selected for further characterization in the established RBM proteolysis FRET assay: S494P, E484K, and L452R (Figure 7A). These mutations correspond to VOCs Alpha B.1.17 (S494P), Beta/Gamma (E484K), and Delta (L452R). RBM1 and RBM2 variant sequences were again synthesized as quenched fluorescent peptides to assess the reactivity of these altered peptide epitopes. While affinity-purified CCP3 IgG proteolyzed the RBM1 epitope containing a. L452R mutation with a velocity comparable to the wildtype peptide sequence, E484K and S494P (RBM2) mutations were completely unreactive in the FRET assay (Figure 7B and Table S4). Next, rRBDs of the corresponding variants were subjected to the same immunoblot proteolysis analysis as before. In contrast to the reactivity pattern observed in variant

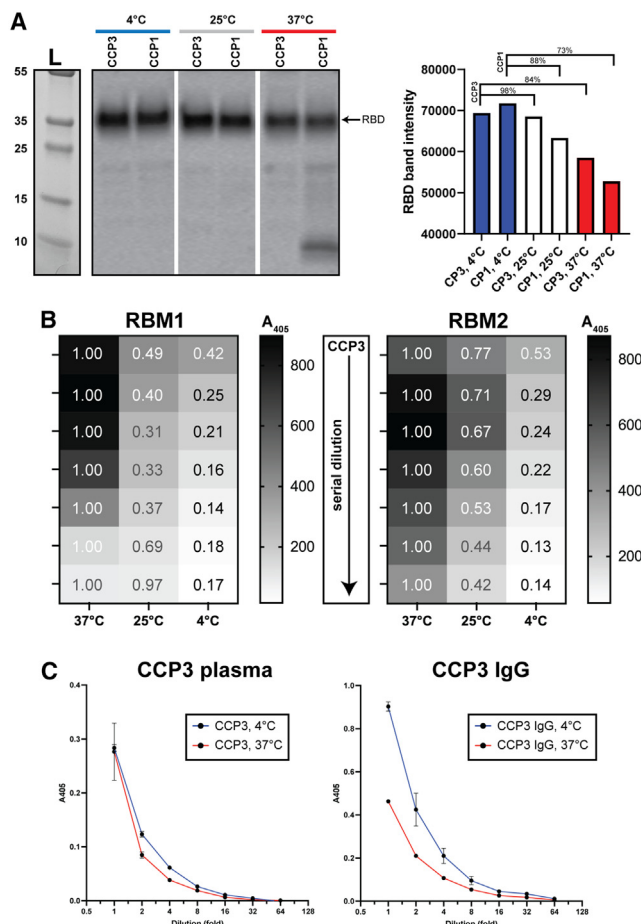


Figure 5. Temperature dependence of RBD proteolysis by CCP enables separation of binding and catalysis

(A) Recombinant RBD was incubated with affinity-purified IgG from two different CP donors (CCP1 and CCP3) for 7 days at three different temperatures, and the reactions were visualized by immunoblot. The RBD band intensities were quantified and compared for each digestion reaction at each temperature. Molecular weight ladders from the aligned Commassie-stained gels are shown for reference and labeled with L.

(B) Quenched fluorescent RBM epitope peptides were incubated with serially diluted, complement-treated CCP3 antibody for 16 h and endpoint fluorescence was measured to assess peptide cleavage. Each reaction was run in duplicate on separate plates which were incubated for the same time at 4, 25, or 37°C. The average total endpoint peptide cleavage observed across all dilutions at 25°C and 4°C was 0.51- and 0.22-fold of that seen at 37°C, respectively for RBM1, and 0.59- and 0.25-fold for RBM2. Fluorescence values, normalized to 37°C at each dilution, are labeled in each cell.

(C) CCP binding of rRBD is comparable at 4 or 37°C. Antibody binding at the two different temperatures was measured by indirect ELISA, where heat-treated CCP3 (left) or purified IgG from CCP3 were incubated with RBD substrates at the two temperatures and binding efficiency was measured. Measured absorbance values at 405 nm as plotted as the mean \pm S.D. of 2 replicates with respect to dilution of serum or antibody.

peptides, the degree of CCP3 antibody proteolysis of each corresponding variant rRBD domain was equivalent, or even greater, to that of the wild-type rRBD (Figure 7C). However, the relative reduction in band intensity of variant rRBDs incubated without antibody suggested that variant rRBDs, especially Omicron rRBD, have intrinsically lower thermostability.

DISCUSSION

Our study demonstrates that antibodies in CCP exhibit proteolytic activity specific to the S protein of SARS-CoV-2, contributing to their antiviral function. Using peptide substrates derived from the RBM epitope of the RBD of SARS-CoV-2, an FRET screen was established to rapidly screen CCP for epitope cleavage. We demonstrated that cleavage is an antibody-mediated process by measuring the proteolytic capacity of CCP, heat-treated plasma, and affinity-purified IgG derived from CCP. The RBM2 epitope (40% of the ACE2 interface) was almost 2-fold as reactive as RBM1 (Class II nAb interface and partial ACE2 interface). Interestingly, the α -RBD IgG concentrations in the four CCP units in our initial screen did not correlate well with proteolytic efficiency, as we observed that samples with very low α -RBD titers demonstrated measurable cleavage of both RBM epitopes. However, several lines of evidence strongly suggest that RBD-specific antibodies drive the observed proteolysis. First, the relative cleavage of epitope probes by CCP IgG compared to nonimmune IgG was significantly faster. Second, the depletion of specific antibody from plasma resulted in significant reductions in cleavage velocity, despite the very low fraction of specific antibody in the total Ig pool. We also saw a weak but significant correlation between RBM1 cleavage and RBD-specific titers in our second CCP library and no correlation for RBM2. The lack of strong correlation could be partially explained by the specific probes used in this study, which only report on cleavage at two specific RBD epitopes. Catalytic activity of α -RBD Abs recognizing alternative epitopes, or conformational epitopes contained within the probe sequences, is not captured by this screen. In particular, the RBM2 sequence features a disulfide linkage which enforces a sharp turn in the peptide backbone in the protein but is absent from the peptide probe.

Further, this could reflect either a greater ratio of antibodies specific to the RBM epitopes used on the screen or a greater ratio of antibodies with catalytic properties, in the low-titer samples. It may also suggest some cross-reactivity of existing antibodies directed against endemic coronavirus.^{47,48} Alternatively, it has been posited that antibodies which undergo positive selection are less likely to be catalytic, as antigenic occupancy of B cell receptors would be reduced if antigen is proteolyzed, thus disfavoring clonal expansion during the B cell differentiation process.^{49–51} Indeed, our findings that nonimmune plasma and depleted plasma still exhibits observable RBD epitope proteolysis suggests that constitutively expressed naive antibodies may account for some nonspecific cleavage. However, the enhancement of RBD cleavage observed in high-titer CCP indicates that proteolytic activity is not completely eliminated in antibodies that undergo affinity maturation, and that greater specificity and titer may enhance the activity of such antibodies compared to naive immunoglobulins.

Analysis of protease inhibitor screen revealed the potent inhibitory effect of the serine protease inhibitor AEBF, suggesting that a large proportion of catalytic antibodies found in CCP3 use cleavage mechanisms similar to conventional serine proteases. A smaller fraction of catalytic antibodies is also inhibited by aminopeptidase inhibitors. Serine protease-like mechanisms for catalytic antibodies have been previously hypothesized, and

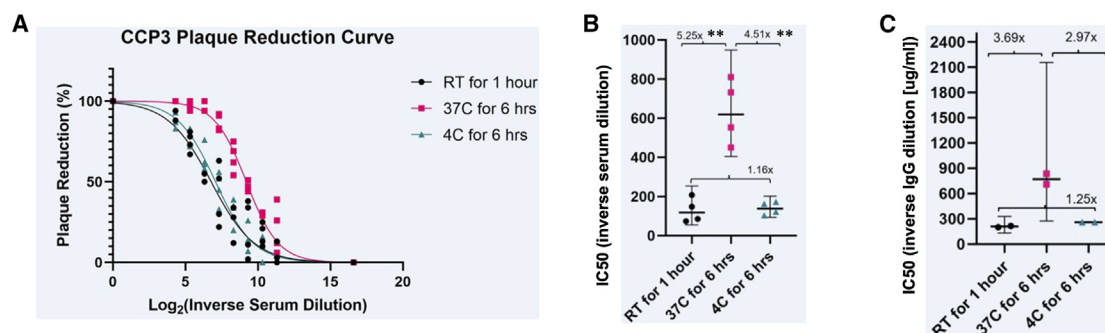


Figure 6. Viral neutralization correlates with antibody-mediated S protein damage

The CCP3 convalescent plasma or purified IgG samples were tested against three different temperatures using A.3 lineage isolates to determine virus neutralization activity.

(A) Serial dilutions of heat-treated plasma were assessed for their ability to inhibit plaque formation, with plaque reduction normalized to no serum controls at the same dilution. IC₅₀ (half maximal inhibitory concentration) was calculated using the inhibition-dose response of plaque reduction over 2-fold serial dilutions of plasma starting from 1:20 using (B) heat-treated CCP3 or (C) purified IgG from CCP3. Geometric mean titer and 95% confidence intervals are indicated and the geometric mean fold drops between temperatures is denoted above each dataset. CCP3 heat-treated plasma and affinity-purified CCP3 IgG were assessed with four and two technical replicates, respectively. Statistical significance was measured using the Mann Whitney matched rank test, **p = 0.0286.

catalytic triads reminiscent of serine protease active sites were identified in nearly a quarter of annotated catalytic antibodies with deposited structures.³² On the other hand, aminopeptidases only cleave at the amino terminus of polypeptide chains, and as such would require an initial cleavage by an endoprotease in order to further degrade the RBD. Interestingly, the aggregate effect of all inhibitors in this screen (57%) would not completely abrogate the activity of CCP3, suggesting that there are additional noncanonical, antibody-specific mechanisms at play that are not attenuated by traditional inhibitors.⁵²

Using purified antibody from a CCP sample with high specific antibody titer and efficient proteolysis kinetics (CCP3), we observed extensive antibody-mediated proteolysis of recombinant S protein domains. Importantly, incubation of authentic SARS-CoV-2 virions with CCP3 IgG likewise resulted in S protein fragmentation. The total extent of CCP3 IgG cleavage of viral S was less than that of recombinant S domains (15% vs. 51–70% degradation of authentic virus and recombinant S1/RBD catalyzed by 1 mg/mL CCP3 IgG). This could be attributable to the β-propiolactone deactivation method used, which can introduce stabilizing crosslinks to the S protein^{52,53} or partial shielding of epitopes in the trimeric S configuration. Regardless, when viral neutralization by CCP3 was directly assessed using a modified PRNT assay, we observed significantly more potent neutralization at the catalysis-permissive temperature compared to the low temperature which permits only antigen binding. Furthermore, antibody-mediated proteolysis of the S protein appears to be a widespread phenomenon, as we observed RBM proteolysis across two large libraries of CCP and measured a correlation between antibody neutralization capacity and proteolytic efficiency of RBM epitopes. We note that this correlation may be improved if the extended antibody incubation time employed in this study (to allow for more extensive antigen cleavage) was used in the original virus neutralization measurements of the library. Additionally, our observation of an inverse correlation between proteolysis and donor age is intriguing because younger patients generally do not exhibit severe COVID-19 symptoms.^{54,55}

Antibody-mediated proteolysis must necessarily work in concert with conventional blocking mAbs to exert relevant influence on the neutralization process. As antibody neutralization by blocking works on the order of minutes,^{56,57} the kinetics of S protein damage measured *in vitro* might at first glance seem too slow to contribute meaningfully to neutralization on the same timescale. However, while the kinetics of this process are slow compared to traditional proteases, these activities can exert significant immunological effects *in vivo*, given the long half-life and high titers of antibodies in circulation³¹ and considering that the amount of viral substrate relative to catalyst is quite low compared to the substrate concentrations processed natural enzymes. By extrapolating the *in vitro* proteolysis kinetics measured in this study, we calculated that every S protein in the human body at peak viral load could be proteolyzed within seconds assuming complete substrate accessibility (see Note S1 for detailed kinetics argument). Indeed, our *in vitro* PRNT data indicates that IC₅₀ for CCP3 decreases 4.5- to 3-fold when proteolysis is inhibited in heat-treated plasma or purified IgG, respectively. Hence, 67–78% of the virus was neutralized via proteolysis in catalytic conditions, as only 22–33% of the antibody was required to achieve IC₅₀ values equivalent to the same antibody in catalysis-inhibited conditions.

An even more important role of antibody-mediated proteolysis may be in the destruction of epitopes undergoing antigenic drift, such as variant viral proteins. As such, we were particularly interested if S protein substitutions from important VOC escaped the proteolytic activity of CCP antibodies elicited before variant emergence. When RBM variant peptides were analyzed, no measurable cleavage was observed when S494P and E484K substitutions were introduced, likely due to abrogation of binding affinity for these altered peptide epitopes. This finding also provides further evidence that catalytic antibodies have a high degree of specificity to their cognate epitopes. However, the CCP antibody did cleave the Delta variant RBM peptide (L452R) with comparative efficiency to the wild-type sequence, implying CCP-mediated proteolysis does not rely on the leucine at this position for recognition. Therefore, at the peptide level,

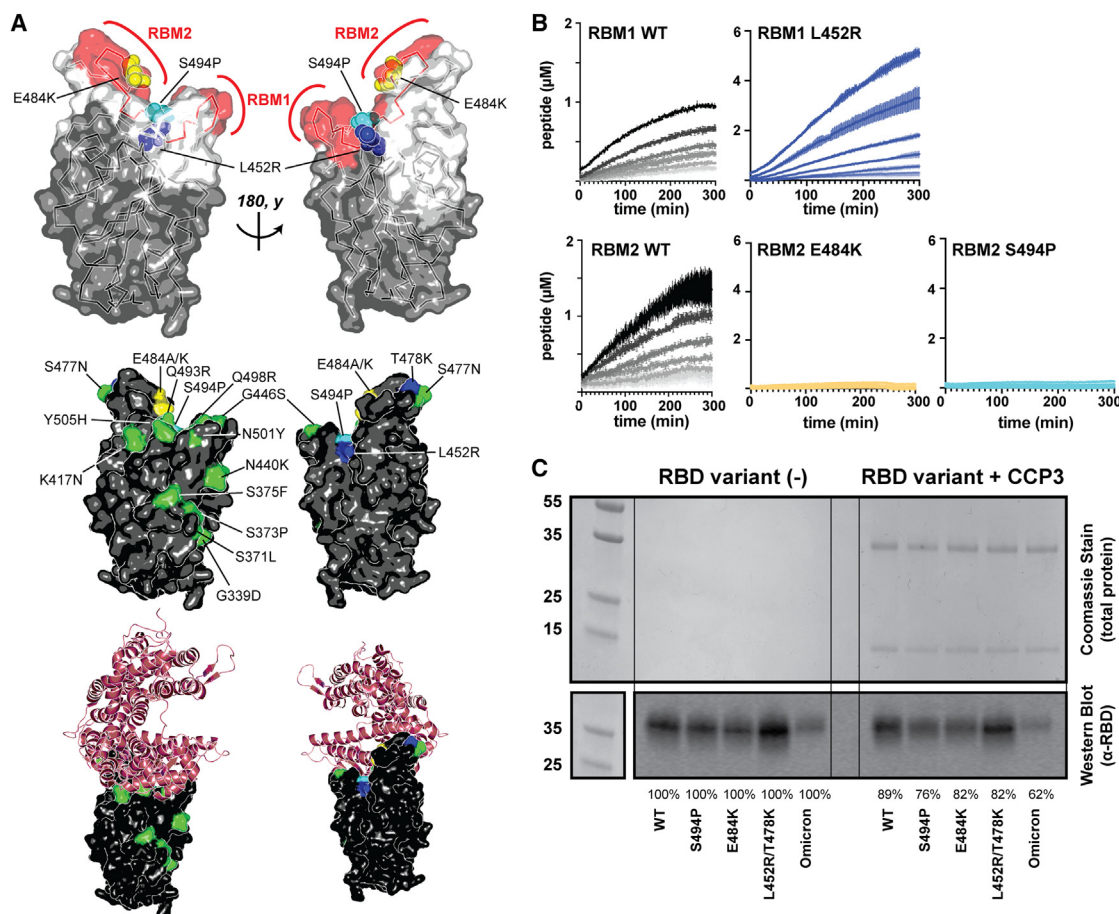


Figure 7. Antibody-mediated S protein epitope cleavage for VOC

The susceptibility to antibody-mediated cleavage of quenched fluorescent peptides encoding amino acid substitutions within the RBM1 and RBM2 sequences found in VOC was determined by measurement of fluorescence over time. (A, top) The location of the mutations of interest on the structure of RBD are highlighted as spheres and colored dark blue, yellow, and cyan for L452R, E484K, and S494P substitutions, respectively. The RBD is displayed as dark gray surface representation and RBM1 and RBM2 peptide epitope locations are highlighted in red, and the entire RBM is colored white. (A, middle) RBD is displayed in the same orientation as the top panel and colored dark gray. Alpha substitutions are highlighted in cyan, Beta/Gamma substitutions in yellow, Delta substitutions in dark blue, and Omicron BA.1 substitutions in green. (A, bottom) The RBD with the same color scheme and orientation as above is displayed in complex with ACE2 (PDB 6M0J).

(B) Kinetic FRET traces observed when purified CCP3 IgG at concentrations ranging from 10 mg/mL to 156 μg/mL was incubated with each variant RBM FRET peptide for 5 h. See Table S4 for full proteolytic kinetics of variant RBM peptides. Each kinetic curve is displayed the mean ± S.D. of 2 replicates, and fluorescence measurements were converted to units of molarity of proteolyzed peptide epitope using each corresponding positive control.

(C) Antibody-mediated proteolysis of recombinant RBD.

protein with S494P, E484K, L452R/T478K, or Omicron substitutions is compared to proteolysis of wild-type recombinant RBD. Recombinant RBD (10 μg/mL) was incubated with CCP3 IgG (500 μg/mL) or alone at 37°C for 7 days. Band intensities of RBD following the incubation period, normalized to the corresponding sample at time zero, are labeled for each digestion reaction. Molecular weight ladders from the aligned Coomassie-stained gels are shown for reference and labeled with L.

certain residues in the S sequence are critical for recognition and proteolysis, while other mutations can be tolerated, likely due to the relative prevalence of certain epitopes targeted by the polyclonal antibody population. Conversely, on the level of S protein domains, we observed that rRBD variants were degraded even more efficiently than the wild-type RBD. Cleavage of Beta/Gamma and Delta rRBD, but not the corresponding RBM peptides is not unexpected, given that the RBM epitopes comprise only a small subset of the total available RBD epitopes, many of which are likely cleaved by cross-reactive catalytic antibodies specific to conserved epitopes in CCP. Conversely, the

enhancement of variant rRBD degradation with respect to wild-type protein was surprising. Paradoxically, while these substitutions are selected for by weakening the binding of non-catalytic antibodies, they may result in RBD structures that are better substrates for catalytic antibodies due to slight structural perturbations which may destabilize the domain and enhance the proteolytic susceptibility of certain epitopes. For example, the heavily mutated Omicron RBD is markedly destabilized, but the destabilization is partially compensated for by additional mutations in S2 or N-terminal domain in the context of the full S ectodomain.^{58,59} While S protein substitutions rapidly weaken

antibody binding and thus neutralization by competitive binding, antibody proteolysis is more durable, perhaps because lower-affinity transient binding events are sufficient to permit proteolysis. In agreement with this model, it was recently reported that CCP from donors never exposed to newer variants can nevertheless neutralize novel SARS-CoV-2 variants.⁶⁰ Further, CCP obtained more recently and from the same geographic community would likely contain S-specific antibody with higher binding affinity to the specific circulating S protein variant.²⁰

Our findings are relevant to the interpretation of results from earlier studies of antibody-mediated viral neutralization, which implicated the destabilization of viral proteins driven by immune complexation with antibodies. Early evidence for viral destabilization by antibodies included the finding that a low proportion of mAbs specific to poliovirus type 1 was capable of “disruptive” neutralization which was irreversible by dissolution of the immune complexes and resulted in the release of genetic material from the virion.^{61,62} Two separate groups also reported that a single neutralizing antibody was sufficient to neutralize 2–4 receptor proteins in influenza and flavivirus.^{63,64} In the light of antibody-mediated viral proteolysis reported here, one could imagine that catalytic turnover may account for the non-stoichiometric neutralizing capacity exerted by each antibody in those studies. More recently, neutralizing antigen-binding fragments (Fabs) were shown to completely dissociate the envelope glycoprotein gp120 trimer of human immunodeficiency virus type-1 into smaller fragments, which were shed from the virion.⁶⁵ Although not specifically implicated, antibody-mediated proteolysis could explain that destabilization. In a separate study, the generation of proteolytic fragments of gp120 catalyzed by purified IgM and IgA was directly observed using biotinylated substrates.^{49,66} Catalysis by natural antibodies is not limited to viral epitopes, as cleavage of *Staphylococcus aureus* extracellular fibrinogen-binding protein (Efb) has also been reported.⁵¹ These studies are consistent with the notion that antibody-mediated catalytic damage of important microbial virulence factors is likely a common occurrence.

Limitations of the study

In this study, proteolysis screening of CCP libraries was limited to the peptide epitopes selected. RBM1 and RBM2 peptides were adopted based on coverage of common epitopes of known neutralizing antibodies as well as the known functional importance to the interaction of the spike protein with the ACE2 receptor. Inclusion of additional peptide sequences derived from spike, including non-neutralizing epitopes, would provide information about the contribution of antibody proteolysis to neutralization for other domains within S1 or S2 subunits. Expansion of the epitope probe library could capture more of the total catalysis performed by CCP antibodies and is likely to improve the statistical correlations between catalytic activity and neutralization titers for each CCP unit. Further, the use of peptides as cleavage targets may underestimate the total cleavage of a particular Spike region if antibodies recognize conformational epitopes within that sequence. Additionally, though we focused our *in vitro* characterization of antibody catalysis on IgG derived from CCP in this study, it is plausible that antibodies of other isotypes also contribute to the overall catalysis. In this regard, we note that much of the viral neutralization capacity of CCP resides

in the IgM and IgG fractions, the former of which was not specifically evaluated in this study. This analysis was limited to the bulk properties of polyclonal CCP Abs, a small fraction of which are specific to spike. Within the specific Ab fraction, it is plausible that only rare mAbs are responsible for catalytic activity. Analysis of monoclonal Abs could address this question and establish critical determinants of specific paratope or epitope sequences that enable antibody catalysis.

SIGNIFICANCE

Traditionally, antibody-mediated viral neutralization is thought to occur by passive binding mechanisms. Antibodies can directly interfere with critical viral processes such as host receptor binding, conformational changes associated with membrane fusion, or the release of viral genome into the cytoplasm. Antibodies also indirectly recruit complement or effector cells to clear circulating virions.^{67,68} However, our finding that antibody-mediated proteolysis of the receptor-engaging machinery of SARS-CoV-2 is associated with virus neutralization implies an additional active role for immunoglobulins in combating viral infections. For example, low-affinity antibodies with significant off-rates have limited neutralization potency due to the reduced timescale of competitive blocking. However, if proteolysis occurs before dissociation, viral deactivation is achieved via irreversible destabilization of viral virulence factors. Furthermore, whereas non-catalytic antibodies deactivate virus stoichiometrically, catalytic antibodies can turn over and cleave multiple molecules per antibody paratope, thus amplifying their potency. Finally, catalytic antibodies which recognize non-neutralizing epitopes can still directly impact neutralization by destabilizing the S protein tertiary and quaternary structure and would not be limited by the conformational shielding of the important epitopes, such as the RBM. Taken together, we predict that antibody-mediated catalysis is an immunologically relevant feature of the humoral immune response which works in concert with conventional antiviral activities of antibodies. Our findings suggest that characterization of the catalytic capacity of convalescent plasma or monoclonal antibodies could provide insights into an additional axis of antibody attributes that drives viral protection.

STAR★METHODS

Detailed methods are provided in the online version of this paper and include the following:

- **KEY RESOURCES TABLE**
- **RESOURCE AVAILABILITY**
 - Lead contact
 - Materials availability
 - Data and code availability
- **EXPERIMENTAL MODEL AND STUDY PARTICIPANT DETAILS**
 - Human subjects
 - Viral strains
 - Cell lines

● **METHOD DETAILS**

- Purification of antibodies from CCP
- FRET assay
- RBD-specific antibody depletion from CCP
- Degradation assay of recombinant S1 or RBD recombinant protein
- Indirect enzyme-linked immunosorbent assays
- Virus inactivation procedure
- Plaque reduction neutralization test (PRNT) assay

● **QUANTIFICATION AND STATISTICAL ANALYSIS**

- Statistical analysis

SUPPLEMENTAL INFORMATION

Supplemental information can be found online at <https://doi.org/10.1016/j.chembiol.2023.05.011>.

ACKNOWLEDGMENTS

We would like to thank Dr. Alan Scott for critical review of this manuscript. National Institutes of Health grants AI052733, AI152078, and HL059842 (A.C.). National Institutes of Health grants T32AI007417 and R01AI162381 (S.A.M.). National Institute of Allergy and Infectious Diseases contract N272201400007C (A.P. and J.S.). U.S. Department of Defense's (DOD) Joint Program Executive Office for Chemical, Biological, Radiological and Nuclear Defense (JPEO-CBRND), in collaboration with the Defense Health Agency (DHA) contract number: W911QY2090012, with additional support from Bloomberg Philanthropies and State of Maryland (D.J.S., E.M.B., and A.A.R.T.). National Heart, Lung, and Blood Institute grant 1K23HL15182 (E.M.B.).

AUTHOR CONTRIBUTIONS

Conceptualization, S.A.M., M.P.W., and A.C.; Methodology, S.A.M.; Investigation, S.A.M., J.S., N.J.M., and P.A.F.; Writing – Original Draft, S.A.M.; Writing – Review and Editing, R.J.B.C., M.P.W., A.A.R.T., E.M.B., D.S., A.P., and A.C.; Resources, A.A.R.T., D.S., A.P., J.R.S., H-S.P., and S.L.K.; Supervision, A.A.R.T., A.P., and A.C.

DECLARATION OF INTERESTS

None declared.

Received: November 18, 2022

Revised: March 23, 2023

Accepted: May 26, 2023

Published: June 23, 2023

REFERENCES

1. Hu, B., Guo, H., Zhou, P., and Shi, Z.L. (). Characteristics of SARS-CoV-2 and COVID-19. *Nat. Rev. Microbiol.* 19, 141–154. <https://doi.org/10.1038/s41579-020-00459-7>.
2. Zhou, P., Yang, X., Lou Wang, X.G., Hu, B., Zhang, L., Zhang, W., Si, H.R., Zhu, Y., Li, B., Huang, C.L., et al. (). A pneumonia outbreak associated with a new coronavirus of probable bat origin. *Nature* 579, 270–273. <https://doi.org/10.1038/s41586-020-2012-7>.
3. Wrapp, D., Wang, N., Corbett, K.S., Goldsmith, J.A., Hsieh, C.-L., Abiona, O., Graham, B.S., and McLellan, J.S. (). Cryo-EM structure of the 2019-nCoV spike in the prefusion conformation. *Science* 367, 1260–1263. <https://doi.org/10.1126/science.abb2507>.
4. Pallesen, J., Wang, N., Corbett, K.S., Wrapp, D., Kirchdoerfer, R.N., Turner, H.L., Cottrell, C.A., Becker, M.M., Wang, L., Shi, W., et al. (). Immunogenicity and structures of a rationally designed prefusion MERS-CoV spike antigen. *Proc. Natl. Acad. Sci. USA* 114, E7348–E7357. <https://doi.org/10.1073/PNAS.1707304114>.
5. Gui, M., Song, W., Zhou, H., Xu, J., Chen, S., Xiang, Y., and Wang, X. (). Cryo-electron microscopy structures of the SARS-CoV spike glycoprotein reveal a prerequisite conformational state for receptor binding. *Cell Res.* 27, 119–129. <https://doi.org/10.1038/cr.2016.152>.
6. Walls, A.C., Xiong, X., Park, Y.-J., Tortorici, M.A., Snijder, J., Quispe, J., Cameroni, E., Gopal, R., Dai, M., Lanzavecchia, A., et al. (). Unexpected receptor functional mimicry elucidates activation of coronavirus fusion. *Cell* 176, 1026–1039.e15. <https://doi.org/10.1016/j.cell.2018.12.028>.
7. Yan, R., Zhang, Y., Li, Y., Xia, L., Guo, Y., and Zhou, Q. (). Structural basis for the recognition of SARS-CoV-2 by full-length human ACE2. *Science* 367, 1444–1448. <https://doi.org/10.1126/SCIENCE.ABB2762>.
8. Xia, S., Zhu, Y., Liu, M., Lan, Q., Xu, W., Wu, Y., Ying, T., Liu, S., Shi, Z., Jiang, S., et al. (). Fusion mechanism of 2019-nCoV and fusion inhibitors targeting HR1 domain in spike protein. *Cell. Mol. Immunol.* 17, 765–767. <https://doi.org/10.1038/s41423-020-0374-2>.
9. Shang, J., Wan, Y., Luo, C., Ye, G., Geng, Q., Auerbach, A., and Li, F. (). Cell entry mechanisms of SARS-CoV-2. *Proc. Natl. Acad. Sci. USA* 117, 11727–11734. <https://doi.org/10.1073/pnas.2003138117>.
10. Rossi, G.A., Sacco, O., Mancino, E., Cristiani, L., and Midulla, F. (). Differences and similarities between SARS-CoV and SARS-CoV-2: spike receptor-binding domain recognition and host cell infection with support of cellular serine proteases. *Infection* 48, 665–669. <https://doi.org/10.1007/S15010-020-01486-5>.
11. Grant, O.C., Montgomery, D., Ito, K., and Woods, R.J. (). Analysis of the SARS-CoV-2 spike protein glycan shield reveals implications for immune recognition. *Sci. Rep.* 10, 14991. <https://doi.org/10.1038/s41598-020-71748-7>.
12. Baden, L.R., el Sahly, H.M., Essink, B., Kotloff, K., Frey, S., Novak, R., Diemert, D., Spector, S.A., Rouphael, N., Creech, C.B., et al. (). Efficacy and safety of the mRNA-1273 SARS-CoV-2 vaccine. *N. Engl. J. Med. Overseas. Ed.* 384, 403–416. <https://doi.org/10.1056/nejmoa2035389>.
13. Polack, F.P., Thomas, S.J., Kitchin, N., Absalon, J., Gurtman, A., Lockhart, S., Perez, J.L., Pérez Marc, G., Moreira, E.D., Zerbini, C., et al. (). Safety and efficacy of the BNT162b2 mRNA covid-19 vaccine. *N. Engl. J. Med.* 383, 2603–2615. <https://doi.org/10.1056/NEJMoa2034577>.
14. Gottlieb, R.L., Nirula, A., Chen, P., Boscia, J., Heller, B., Morris, J., Huhn, G., Cardona, J., Mocherla, B., Stosor, V., et al. (). Effect of bamlanivimab as monotherapy or in combination with etesevimab on viral load in patients with mild to moderate COVID-19: a randomized clinical trial. *JAMA* 325, 632–644. <https://doi.org/10.1001/JAMA.2021.0202>.
15. Weinreich, D.M., Sivapalasingam, S., Norton, T., Ali, S., Gao, H., Bhore, R., Musser, B.J., Soo, Y., Rofail, D., Im, J., et al. (). REGN-COV2, a neutralizing antibody cocktail, in outpatients with covid-19. *N. Engl. J. Med.* 384, 238–251. <https://doi.org/10.1056/NEJMoa2035002>.
16. Gupta, A., Gonzalez-Rojas, Y., Juarez, E., Crespo Casal, M., Moya, J., Falci, D.R., Sarkis, E., Solis, J., Zheng, H., Scott, N., et al. (). Early treatment for covid-19 with SARS-CoV-2 neutralizing antibody sotrovimab. *N. Engl. J. Med.* 385, 1941–1950. <https://doi.org/10.1056/NEJMoa2107934>.
17. Focosi, D., Maggi, F., Franchini, M., McConnell, S., and Casadevall, A. (). Analysis of immune escape variants from antibody-based therapeutics against COVID-19: a systematic review. *Int. J. Mol. Sci.* 23, 29. <https://doi.org/10.3390/IJMS23010029>.
18. Harvey, W.T., Carabelli, A.M., Jackson, B., Gupta, R.K., Thomson, E.C., Harrison, E.M., Ludden, C., Reeve, R., Rambaut, A., COVID-19 Genomics UK COG-UK Consortium, et al. (). SARS-CoV-2 variants, spike mutations and immune escape. *Nat. Rev. Microbiol.* 19, 409–424. <https://doi.org/10.1038/s41579-021-00573-0>.
19. Casadevall, A., Pirofski, L.A., and Joyner, M.J. (). The principles of antibody therapy for infectious diseases with relevance for COVID-19. *mBio* 12, 03372–20. <https://doi.org/10.1128/MBIO.03372-20>.
20. Casadevall, A., Henderson, J.P., Joyner, M.J., and Pirofski, L.A. (). SARS-CoV-2 variants and convalescent plasma: reality, fallacies, and opportunities. *J. Clin. Invest.* 131, e148832. <https://doi.org/10.1172/JCI148832>.

21. Tobian, A.A.R., Cohn, C.S., and Shaz, B.H. (). COVID-19 Convalescent plasma. *Blood* 140, 196–207. <https://doi.org/10.1182/BLOOD.2021012248>.
22. Bloch, E.M., Shoham, S., Casadevall, A., Sachais, B.S., Shaz, B., Winters, J.L., Van Buskirk, C., Grossman, B.J., Joyner, M., Henderson, J.P., et al. (). Deployment of convalescent plasma for the prevention and treatment of COVID-19. *J. Clin. Invest.* 130, 2757–2765. <https://doi.org/10.1172/JCI138745>.
23. Bar, K.J., Shaw, P.A., Choi, G.H., Aquil, N., Fesnak, A., Yang, J.B., Soto-Calderon, H., Grajales, L., Starr, J., Andronov, M., et al. (). A randomized controlled study of convalescent plasma for individuals hospitalized with COVID-19 pneumonia. *J. Clin. Invest.* 131, e155114. <https://doi.org/10.1172/JCI155114>.
24. Estcourt, L.J., Turgeon, A.F., McQuilten, Z.K., McVerry, B.J., Al-Beidh, F., Annane, D., Arabi, Y.M., Arnold, D.M., Beane, A., Bégin, P., et al. (). Effect of convalescent plasma on organ support-free days in critically ill patients with COVID-19: a randomized clinical trial. *JAMA* 326, 1690–1702. <https://doi.org/10.1001/JAMA.2021.18178>.
25. Libster, R., Pérez Marc, G., Wappner, D., Coviello, S., Bianchi, A., Braem, V., Esteban, I., Caballero, M.T., Wood, C., Berrueta, M., et al. (). Early high-titer plasma therapy to prevent severe covid-19 in older adults. *N. Engl. J. Med.* 384, 610–618. <https://doi.org/10.1056/NEJMoa2033700>.
26. Estcourt, L.J., Cohn, C.S., Pagano, M.B., Iannizzi, C., Kreuzberger, N., Skoetz, N., Allen, E.S., Bloch, E.M., Beaudoin, G., Casadevall, A., et al. (). Clinical practice guidelines from the association for the advancement of blood and biotherapies (AABB): COVID-19 convalescent plasma. *Ann. Intern. Med.* 175, 1310–1321.
27. Sullivan, D.J., Gebo, K.A., Shoham, S., Bloch, E.M., Lau, B., Shenoy, A.G., Mosnaim, G.S., Gniadek, T.J., Fukuta, Y., Patel, B., et al. (). Early outpatient treatment for covid-19 with convalescent plasma. *N. Engl. J. Med.* 386, 1700–1711. <https://doi.org/10.1056/NEJMoa2119657>.
28. Bonny, T.S., Patel, E.U., Zhu, X., Bloch, E.M., Grabowski, M.K., Abraham, A.G., Littlefield, K., Shrestha, R., Benner, S.E., Laeyendecker, O., et al. (). Cytokine and chemokine levels in coronavirus disease 2019 convalescent plasma. *Open Forum Infect. Dis.* 8, ofaa574. <https://doi.org/10.1093/OFID/OFAA574>.
29. Natarajan, H., Crowley, A.R., Butler, S.E., Xu, S., Weiner, J.A., Bloch, E.M., Littlefield, K., Wieland-Alter, W., Connor, R.I., Wright, P.F., et al. (). Markers of polyfunctional SARS-CoV-2 antibodies in convalescent plasma. *mBio* 12, 00765–21. <https://doi.org/10.1128/mBio.00765-21>.
30. Crawford, C.J., Wear, M.P., Smith, D.F.Q., d'Errico, C., McConnell, S.A., Casadevall, A., and Oscarson, S. (). A glycan FRET assay for detection and characterization of catalytic antibodies to the *Cryptococcus neoformans* capsule. *Proc. Natl. Acad. Sci. USA* 118, e2016198118. <https://doi.org/10.1073/PNAS.2016198118>.
31. Bowen, A., Wear, M., and Casadevall, A. (). Antibody-mediated catalysis in infection and immunity. *Infect. Immun.* 85, e00202–17. <https://doi.org/10.1128/IAI.00202-17>.
32. Bowen, A., Wear, M.P., Cordero, R.J.B., Oscarson, S., and Casadevall, A. (). A monoclonal antibody to *Cryptococcus neoformans* glucuronoxylomannan manifests hydrolytic activity for both peptides and polysaccharides. *J. Biol. Chem.* 292, 417–434. <https://doi.org/10.1074/JBC.M116.767582>.
33. Paul, S., Volle, D.J., Beach, C.M., Johnson, D.R., Powell, M.J., and Massey, R.J. (). Catalytic hydrolysis of vasoactive intestinal peptide by human autoantibody. *Science* 244, 1158–1162. <https://doi.org/10.1126/SCIENCE.2727702>.
34. Ju, B., Zhang, Q., Ge, J., Wang, R., Sun, J., Ge, X., Yu, J., Shan, S., Zhou, B., Song, S., et al. (). Human neutralizing antibodies elicited by SARS-CoV-2 infection. *Nature* 584, 115–119. <https://doi.org/10.1038/s41586-020-2380-z>.
35. Chakraborti, S., Prabakaran, P., Xiao, X., and Dimitrov, D.S. (). The SARS coronavirus S glycoprotein receptor binding domain: fine mapping and functional characterization. *Virology* 2, 73. <https://doi.org/10.1186/1743-422X-2-73>.
36. Lan, J., Ge, J., Yu, J., Shan, S., Zhou, H., Fan, S., Zhang, Q., Shi, X., Wang, Q., Zhang, L., et al. (). Structure of the SARS-CoV-2 spike receptor-binding domain bound to the ACE2 receptor. *Nature* 581, 215–220. <https://doi.org/10.1038/s41586-020-2180-5>.
37. Yuan, M., Liu, H., Wu, N.C., and Wilson, I.A. (). Recognition of the SARS-CoV-2 receptor binding domain by neutralizing antibodies. *Biochem. Biophys. Res. Commun.* 538, 192–203. <https://doi.org/10.1016/j.BBRC.2020.10.012>.
38. Finkelstein, M.T., Mermelstein, A.G., Miller, E.P., Seth, P.C., Stancovski, E.S.D., and Fera, D. (). Structural analysis of neutralizing epitopes of the SARS-CoV-2 spike to guide therapy and vaccine design strategies. *Viruses* 13, 134. <https://doi.org/10.3390/V13010134>.
39. Deshpande, A., Harris, B.D., Martinez-Sobrido, L., Koble, J.J., and Walter, M.R. (). Epitope classification and RBD binding properties of neutralizing antibodies against SARS-CoV-2 variants of concern. *Front. Immunol.* 12, 2185. <https://doi.org/10.3389/FIMMU.2021.691715/BIBTEX>.
40. Klein, S.L., Pekosz, A., Park, H.-S., Ursin, R.L., Shapiro, J.R., Benner, S.E., Littlefield, K., Kumar, S., Naik, H.M., Betenbaugh, M.J., et al. (). Sex, age, and hospitalization drive antibody responses in a COVID-19 convalescent plasma donor population. *J. Clin. Invest.* 130, 6141–6150. <https://doi.org/10.1172/JCI142004>.
41. Neisser, M., and Wechsberg, F. (). Ueber die Wirkungsart bactericider sera. *Munchner Medizinische Wochenschrift* 48, 697.
42. Bayne-Jones, S. (). Equilibria in precipitin reactions. *J. Exp. Med.* 25, 837–853. <https://doi.org/10.1084/jem.25.6.837>.
43. Weinstock, C., and Schnaidt, M. (). The complement-mediated prozone effect in the Luminex single-antigen bead assay and its impact on HLA antibody determination in patient sera. *Int. J. Immunogenet.* 40, 171–177. <https://doi.org/10.1111/J.1744-313X.2012.01147.X>.
44. Akazawa-Ogawa, Y., Nagai, H., and Hagihara, Y. (). Heat denaturation of the antibody, a multi-domain protein. *Biophys. Rev.* 10, 255–258. <https://doi.org/10.1007/S12551-017-0361-8>.
45. Triglia, R.P., and Linscott, W.D. (). Titers of nine complement components, conglutinin and C3b-inactivator in adult and fetal bovine sera. *Mol. Immunol.* 17, 741–748. [https://doi.org/10.1016/0161-5890\(80\)90144-3](https://doi.org/10.1016/0161-5890(80)90144-3).
46. Hu, X., An, T., Situ, B., Hu, Y., Ou, Z., Li, Q., He, X., Zhang, Y., Tian, P., Sun, D., et al. (). Heat inactivation of serum interferes with the immunoanalysis of antibodies to SARS-CoV-2. *J. Clin. Lab. Anal.* 34, e23411. <https://doi.org/10.1002/JCLA.23411>.
47. Shrock, E., Fujimura, E., Kula, T., Timms, R.T., Lee, I.-H., Leng, Y., Robinson, M.L., Sie, B.M., Li, M.Z., Chen, Y., et al. (). Viral epitope profiling of COVID-19 patients reveals cross-reactivity and correlates of severity. *Science* 370, eabd4250. <https://doi.org/10.1126/science.abd4250>.
48. Yaqinuddin, A. (). Cross-immunity between respiratory coronaviruses may limit COVID-19 fatalities. *Med. Hypotheses* 144, 110049. <https://doi.org/10.1016/J.MEHY.2020.110049>.
49. Planque, S., Mitsuda, Y., Taguchi, H., Salas, M., Morris, M.K., Nishiyama, Y., Kyle, R., Okhuysen, P., Escobar, M., Hunter, R., et al. (). Characterization of gp120 hydrolysis by IgA antibodies from humans without HIV infection. *AIDS Res. Hum. Retroviruses* 23, 1541–1554. <https://doi.org/10.1089/AID.2007.0081>.
50. Polosukhina, D.I., Buneva, V.N., Doronin, B.M., Tyshkevich, O.B., Boiko, A.N., Gusev, E.I., Favorova, O.O., and Nevinsky, G.A. (). Hydrolysis of myelin basic protein by IgM and IgA antibodies from the sera of patients with multiple sclerosis. *Med. Sci. Monit.* 17, BR266–BR272.
51. Brown, E.L., Nishiyama, Y., Dunkle, J.W., Aggarwal, S., Planque, S., Watanabe, K., Csencsits-Smith, K., Bowden, M.G., Kaplan, S.L., and Paul, S. (). Constitutive production of catalytic antibodies to a *Staphylococcus aureus* virulence factor and effect of infection. *J. Biol. Chem.* 287, 9940–9951. <https://doi.org/10.1074/jbc.M111.330043>.
52. Perrin, P., and Morgeaux, S. (). Inactivation of DNA by beta-propiolactone. *Biologicals* 23, 207–211. <https://doi.org/10.1006/BIOL.1995.0034>.
53. Uittenbogaard, J.P., Zomer, B., Hoogerhout, P., and Metz, B. (). Reactions of beta-propiolactone with nucleobase analogues, nucleosides, and

- peptides: implications for the inactivation of viruses. *J. Biol. Chem.* 286, 36198–36214. <https://doi.org/10.1074/JBC.M111.279232>.
54. Zhou, F., Yu, T., Du, R., Fan, G., Liu, Y., Liu, Z., Xiang, J., Wang, Y., Song, B., Gu, X., et al. (). Clinical course and risk factors for mortality of adult inpatients with COVID-19 in Wuhan, China: a retrospective cohort study. *Lancet* 395, 1054–1062. [https://doi.org/10.1016/S0140-6736\(20\)30566-3](https://doi.org/10.1016/S0140-6736(20)30566-3).
55. Kim, L., Garg, S., O'Halloran, A., Whitaker, M., Pham, H., Anderson, E.J., Armistead, I., Bennett, N.M., Billing, L., Como-Sabetti, K., et al. (). Risk factors for intensive care unit admission and in-hospital mortality among hospitalized adults identified through the US coronavirus disease 2019 (COVID-19)-Associated hospitalization surveillance network (COVID-NET). *Clin. Infect. Dis.* 72, E206–E214. <https://doi.org/10.1093/CID/CIAA1012>.
56. McLain, L., and Dimmock, N.J. (). Single- and multi-hit kinetics of immunoglobulin G neutralization of human immunodeficiency virus type 1 by monoclonal antibodies. *J. Gen. Virol.* 75 (Pt 6), 1457–1460. <https://doi.org/10.1099/0022-1317-75-6-1457/CITE/REFWORKS>.
57. Magnus, C. (). Virus neutralisation: new insights from kinetic neutralisation curves. *PLoS Comput. Biol.* 9, e1002900. <https://doi.org/10.1371/JOURNAL.PCBI.1002900>.
58. Stalls, V., Lindenberger, J., Gobeil, S.M.-C., Henderson, R., Parks, R., Barr, M., Deyton, M., Martin, M., Janowska, K., Huang, X., et al. (). Cryo-EM structures of SARS-CoV-2 Omicron BA.2 spike. *Cell Rep.* 39, 111009. <https://doi.org/10.1016/J.CELREP.2022.111009>.
59. Javanmardi, K., Segall-Shapiro, T.H., Chou, C.-W., Boutz, D.R., Olsen, R.J., Xie, X., Xia, H., Shi, P.-Y., Johnson, C.D., Annareddy, A., et al. (). Antibody escape and cryptic cross-domain stabilization in the SARS-CoV-2 Omicron spike protein. *Cell Host Microbe* 30, 1242–1254.e6. <https://doi.org/10.1016/J.CHOM.2022.07.016>.
60. Li, M., Beck, E.J., Laeyendecker, O., Eby, Y., Tobian, A.A.R., Caturegli, P., Wouters, C., Chiklis, G.R., Block, W., McKie, R.O., et al. (). Convalescent plasma with a high level of virus-specific antibody effectively neutralizes SARS-CoV-2 variants of concern. *Blood Adv.* 6, 3678–3683. <https://doi.org/10.1182/BLOODADVANCES.2022007410>.
61. Delaet, I., and Boeyé, A. (). Capsid destabilization is required for antibody-mediated disruption of poliovirus. *J. Gen. Virol.* 75, 581–587. <https://doi.org/10.1099/0022-1317-75-3-581>.
62. Bröen, P., Rombaut, B., and Boeyé, A. (). Hit-and-run neutralization of poliovirus. *J. Gen. Virol.* 66, 2495–2499. <https://doi.org/10.1099/0022-1317-66-11-2495>.
63. Pierson, T.C., and Diamond, M.S. (). A game of numbers: the stoichiometry of antibody-mediated neutralization of flavivirus infection. *Prog. Mol. Biol. Transl. Sci.* 129, 141–166. <https://doi.org/10.1016/BS.PMBTS.2014.10.005>.
64. Taylor, H.P., Armstrong, S.J., and Dimmock, N.J. (). Quantitative relationships between an influenza virus and neutralizing antibody. *Virology* 159, 288–298. [https://doi.org/10.1016/0042-6822\(87\)90466-1](https://doi.org/10.1016/0042-6822(87)90466-1).
65. Lee, J.H., Leaman, D.P., Kim, A.S., Torrents de la Peña, A., Sliepen, K., Yasmeen, A., Derking, R., Ramos, A., De Taeye, S.W., Ozorowski, G., et al. (). Antibodies to a conformational epitope on gp41 neutralize HIV-1 by destabilizing the Env spike. *Nat. Commun.* 6, 8167. <https://doi.org/10.1038/NCOMMS9167>.
66. Paul, S., Karle, S., Planque, S., Taguchi, H., Salas, M., Nishiyama, Y., Handy, B., Hunter, R., Edmundson, A., and Hanson, C. (). Naturally occurring proteolytic antibodies: selective immunoglobulin M-catalyzed hydrolysis of HIV gp120. *J. Biol. Chem.* 279, 39611–39619. <https://doi.org/10.1074/JBC.M406719200>.
67. Klasse, P.J. (). Neutralization of virus infectivity by antibodies: old problems in new perspectives. *Adv. Biol.* 2014, 157895. <https://doi.org/10.1155/2014/157895>.
68. Corti, D., and Lanzavecchia, A. (). Broadly neutralizing antiviral antibodies. *Annu. Rev. Immunol.* 31, 705–742. <https://doi.org/10.1146/annurev-immunol-032712-095916>.
69. Shoham, S., Bloch, E.M., Casadevall, A., Hanley, D., Lau, B., Gebo, K., Cachay, E., Kassaye, S.G., Paxton, J.H., Gerber, J., et al. (). Transfusing convalescent plasma as post-exposure prophylaxis against SARS-CoV-2 infection: a double-blinded, phase 2 randomized, controlled trial. *Clin. Infect. Dis.* 76, e477–e486. <https://doi.org/10.1093/CID/CIAC372>.
70. Patel, E.U., Bloch, E.M., Clarke, W., Hsieh, Y.H., Boon, D., Eby, Y., Fernandez, R.E., Baker, O.R., Keruly, M., Kirby, C.S., et al. (). Comparative performance of five commercially available serologic assays to detect antibodies to SARS-CoV-2 and identify individuals with high neutralizing titers. *J. Clin. Microbiol.* 59, 02257–20. <https://doi.org/10.1128/JCM.02257-20>.
71. Schneider, C.A., Rasband, W.S., and Eliceiri, K.W. (). NIH Image to ImageJ: 25 years of image analysis. *Nat. Methods* 9, 671–675. <https://doi.org/10.1038/NMETH.2089>.
72. Dhakal, S., Ruiz-Bedoya, C.A., Zhou, R., Creisher, P.S., Villano, J.S., Littlefield, K., Ruelas Castillo, J., Marinho, P., Jedlicka, A.E., Ordonez, A.A., et al. (). Sex differences in Lung imaging and SARS-CoV-2 antibody responses in a COVID-19 golden Syrian hamster model. *mBio* 12, e0097421. <https://doi.org/10.1128/MBIO.00974-21>.
73. Gordon, O., Brosnan, M.K., Yoon, S., Jung, D., Littlefield, K., Ganesan, A., Caputo, C.A., Li, M., Morgenlander, W.R., Henson, S.N., et al. (). Pharmacokinetics of high-titer anti-SARS-CoV-2 human convalescent plasma in high-risk children. *JCI Insight* 7, e151518. <https://doi.org/10.1172/JCI.INSIGHT.151518>.

STAR★METHODS

KEY RESOURCES TABLE

REAGENT or RESOURCE	SOURCE	IDENTIFIER
Antibodies		
Polyclonal Rabbit RBD antibody	Sino Biological	Cat#40592-T62; RRID:AB_2927483
Europium-labeled Goat α -Mouse IgG	Molecular Devices	Cat#R8208
HRP-conjugated Goat anti-Rabbit Ig	Southern Biotech	Cat#4010-05; RRID:AB_2632593
Monoclonal Anti-SARS Coronavirus/SARS-Related Coronavirus 2 Spike Glycoprotein Receptor Binding Domain (RBD)	Sino Biological	Cat#40150-D001
Goat α -Human IgG H + L-AP	Southern Biotech	Cat#2040-04;
Bacterial and virus strains		
SARS-CoV-2 clade A.3 isolate SARS-CoV-2/USA/MD-HP00076/2020	Division of Medical Microbiology, Department of Pathology, Johns Hopkins School of Medicine, Baltimore, Maryland, USA	GISAID accession number: EPI_ISL_438234
Biological samples		
Patient convalescent plasma	Johns Hopkins Hospital, Department of Pathology, Transfusion Medicine Division	See Table S5 ^{27,40,69,70}
Chemicals, peptides, and recombinant proteins		
Synthetic quenched fluorescent peptide (RBM1)	Peptide 2.0	[7-methoxycoumarin-4-acetic acid] (Mca) – KVGGNYYNL – K(Dnp) [2,4-dinitrophenyl]
Synthetic quenched fluorescent peptide (RBM2)	Peptide 2.0	[7-methoxycoumarin-4-acetic acid] (Mca) – VEGFNCYFPLQS – K(Dnp) [2,4-dinitrophenyl]
Proteinase K	Invitrogen	Cat#25530049
AEBSF	Thermo Scientific	Cat#78431
Bestatin	Thermo Scientific	Cat#78433
E-64	Thermo Scientific	Cat#78434
Pepstatin-A	Thermo Scientific	Cat#78436
SARS-CoV-2 Spike RBD-coupled magnetic beads	Acro Biosystems	Cat#MBS-K002
Recombinant RBD (wild-type)	Sino Biologicals	Cat#40592-V08H
Recombinant RBD (S494P)	Sino Biologicals	Cat#40592-V08H18
Recombinant RBD (E484K)	Sino Biologicals	Cat#40592-V08H84
Recombinant RBD (L452R/T478K)	Sino Biologicals	Cat#40592-V08H90
Recombinant RBD (Omicron; G339D/S371L/S373P/ S375F/K417N/N440K/G446S/S477N/T478K/E484A/ Q493R/G496S/Q498R/N501Y/Y505H)	Sino Biologicals	Cat#40592-V08H121
Recombinant S1 (wild-type)	Sino Biologicals	Cat#40591-V08H
SuperSignal West Pico PLUS Chemiluminescent Substrate	Fisher Scientific	Cat#34577
para-Nitrophenylphosphate (PNPP)	Sigma-Aldrich	Cat#S0942-100TAB
β -propiolactone	Millipore Sigma	Cat#P5648-1ML
DMEM	Gibco-Thermo Fisher	Cat#11965118
Fetal Bovine Serum	Gibco-Thermo Fisher	Cat#F2442-500ML
Glutamine	Life Technologies	Cat#25030081
Sodium Pyruvate	Sigma	Cat#S8636-100ML

(Continued on next page)

Continued

REAGENT or RESOURCE	SOURCE	IDENTIFIER
Penicillin	Quality Biologicals	Cat#120-095-721
Streptomycin	Quality Biologicals	Cat#120-095-721
Methylcellulose	Sigma-Aldrich	Cat#435244-250G
Critical commercial assays		
NAb Protein A/G spin columns	Thermo Fisher	Cat#89958
4-20% Mini-PROTEAN TGX protein gels	BioRad	Cat#4561096
Immobilon-P transfer membranes	Millipore	Cat#IPVH00010
Bicinchoninic acid assay	Thermo Fisher	Cat#23227
Deposited data		
Raw immunoblot images, raw FRET kinetics data	Mendeley Data	https://doi.org/10.17632/28cft6pz76.2
Experimental models: Organisms/strains		
VeroE6-TMPRSS2	Cell repository of the National Institute of Infectious Diseases, Japan	RRID: CVCL_YQ49
Software and algorithms		
GraphPad Prism	Graphpad Software	https://www.graphpad.com/scientificsoftware/prism/
ImageJ	Schneider et al. ⁷¹	https://imagej.nih.gov/ij/
Adobe Illustrator	Adobe	https://www.adobe.com/
Excel	Microsoft	https://www.microsoft.com/en-us/microsoft-365/excel
BioRender	BioRender	https://biorender.com/
R 4.2.1	R Core Team	https://www.r-project.org/

RESOURCE AVAILABILITY

Lead contact

Further information and requests for resources and reagents should be directed to and will be fulfilled by the lead contact, Arturo Casadevall (acascade1@jhu.edu).

Materials availability

This study did not generate any new unique reagents.

Data and code availability

- Raw FRET kinetics data for de-identified human plasma samples and original western blot images have been deposited at Mendeley and are publicly available as of the date of publication. Additional Supplemental Items available from Mendeley Data at <https://doi.org/10.17632/28cft6pz76.2>.
- This paper does not report original code.
- All data reported in this paper and any additional information required to reanalyze the data reported in this paper is available from the [lead contact](#) upon request.

EXPERIMENTAL MODEL AND STUDY PARTICIPANT DETAILS

Human subjects

The main CCP samples (CCP1-4) were thawed plasma samples from volunteer apheresis convalescent plasma donors obtained in June 2020 from the Transfusion Medicine Division, Department of Pathology at the Johns Hopkins Hospital. The first library of CCP samples was selected at random from a set of 300 recent convalescent plasma donors collected for two clinical trials^{27,69} (see [Table S5](#) for detailed description of each CCP sample). The first donor cohort was composed of 22 (49%) males and 24 (51%) females with a mean age of 46 years. The second library, also collected for clinical trials, consists of 126 highly characterized CCP samples and the principal cohort of the study has been previously described.^{40,70} Briefly, for both the first and second libraries, individuals were previously diagnosed with SARS-CoV-2 infection by PCR+ nasal swab who met the standard eligibility criteria for blood donation and were collected in the Baltimore, MD, and Washington DC area (Johns Hopkins Medical Institutions, JHMI cohort). The

second cohort was composed of 68 (54%) males and 58 (46%) females. 12 (10%) cases were severe enough to require hospitalization (median duration of stay 5 days; interquartile range 2–7 days). Plasma was collected from each donor approximately one month after symptom onset or the first positive PCR test in the case of mild or asymptomatic disease (see Table S5 for detailed description of each CCP sample). Human subject research was approved by both the Johns Hopkins University School of Medicine's Institutional Review Board. Nonimmune plasma samples were randomly selected from leftover control plasma from the early treatment randomized control trial collected in November 2020 and confirmed seronegative.²⁷ All participants provided informed written consent.

Viral strains

SARS-CoV-2 clade A.3 isolate (SARS-CoV-2/USA/MD-HP00076/2020 GISAID accession number EPI_ISL_438234) were used for PRNT or deactivated for use in *in vitro* degradation immunoblot assays.

Cell lines

Female VeroE6-TMPRSS2 were cultured at 37°C with 5% carbon dioxide in a humidified chamber, using complete medium consisting of minimum essential medium (MEM) supplemented with 10% fetal bovine serum, 1 mmol/L glutamine, 1 mmol/L sodium pyruvate, 100 µg/mL penicillin, and 100 µg/mL streptomycin. For each experiment, cells were plated in 6-well dishes and grown to 75% confluence.

METHOD DETAILS

Purification of antibodies from CCP

Polyclonal antibodies from CCP were purified by NAb Protein A/G spin columns (Thermo Fisher) according to the manufacturer's protocols. Purified mAbs were assessed for purity by separation with SDS-PAGE and protein staining with SimplyBlue Coomassie stain (Thermo Fisher). The total mAb concentration was then determined by Beer's Law using absorbance at 280 nm and approximate molar absorptivity coefficients for human IgG. Purified polyclonal antibody mixtures were then heat-treated at 55°C for 30 min and centrifuged at 5000 x g to denature any selectively residual non-antibody biomolecules.

FRET assay

Quenched fluorescent peptides appended with 7-methoxycoumarin-4-acetic acid (Mca) and 2,4-dinitrophenyl (Dnp) at the N-terminus and C-terminal lysine sidechain, respectively, were synthesized by Peptide 2.0. Kinetic assays with the RBD FRET peptides were performed by diluting each antibody with PBS in 40 µL in an opaque microtiter assay plate (Corning 3993). To each well, 10,000–156 µg/mL of purified CCP antibody, 1- to 64-fold dilution of serum was mixed with 75 µM of RBD FRET peptide was added. Fluorescence was measured with excitation and emission wavelengths of 320 and 405 nm, respectively, and an emission cutoff filter at 320 nm, using the SpectraMax M5 plate reader (Molecular Devices) at a constant temperature of 37°C. Wells were set up in duplicate and fluorescence was measured every minute for 5 h, with a 3 s mixing step between reads. The maximal RFU value measured for the positive control proteinase K (Invitrogen; 2 mg/mL) digestion of RBM FRET peptides (PK_{max}) was considered complete peptide cleavage (75 µM) and the ratio of maximal RFU for each condition to PK_{max} was used to calculate total peptide cleavage for each antibody at 200 min, which was then used to calculate initial velocity. For the protease inhibitor screen, the assay set up was identical except for the supplementation of AEBSF (Thermo Scientific), bestatin (Thermo Scientific), E-64 (Thermo Scientific), and pepstatin-A (Thermo Scientific) at constant working concentrations of 1 mM, 40 µM, 10 µM, and 1.5 µM, respectively. For inhibitors dissolved in organic solvents (E-64, 50% EtOH; bestatin and pepstatin-A, 100% MeOH), an equivalent amount of the carrier solvent was supplemented to proteolysis reactions without inhibitor as control.

RBD-specific antibody depletion from CCP

SARS-CoV-2 Spike RBD-coupled magnetic beads (Acro Biosystems) were incubated with heat-treated CCP3 plasma overnight at 4°C with gentle rotation. The magnetic beads were then separated from the CCP3 using a magnetic separator, and the supernatant (containing RBD-specific Ab-depleted plasma) was removed. The efficiency of RBD-specific antibody removal was assessed by ELISA.

Degradation assay of recombinant S1 or RBD recombinant protein

Recombinant proteins were obtained from Sino Biologicals and reconstituted in sterile water at 0.25 mg/mL. RBD constructs contained SARS-CoV-2 amino acid sequence from R319-F541 and a C-terminal polyhistidine tags. The spike S1 construct contained SARS-CoV-2 S protein amino acid sequence Val¹⁶-Arg⁶⁸⁵ and a C-terminal polyhistidine tag. Recombinant S1 subunit or RBD was dissolved in 1XDPBS at a concentration of 50 or 10 µg/mL, respectively. Antibody was added to the reactions at concentrations ranging from 125 to 2000 µg/mL and the reactions were incubated at 37°C with rotation for a period of up to 7 days. The reactions were then separated under reducing conditions using 4–20% Mini-PROTEAN TGX protein gels (BioRad) and transferred to Immobilon-P transfer membranes (Millipore) in transfer buffer (20% methanol, 48 mM Tris, 39 mM Glycine, 0.00375% SDS (Sodium Dodecyl Sulfate)) for 10 min at 1.3 A and 25V using a Trans-Blot Turbo Transfer System (BioRad). The membranes were then blocked with 5% BSA (Bovine Serum Albumin) + 0.1% TWEEN 20 for 1 h and blotted with primary antibody overnight at 4°C in blocking solution. The membranes were then washed 5x with TBST (Tris, NaCl, 0.1% TWEEN 20) and probed with a secondary antibody for 1 h at

37°C with gentle shaking. Polyclonal Rabbit anti-RBD antibody (Sino Biological) was employed as the primary antibody, and Europium-labeled Goat α -Mouse IgG (Molecular Devices) or HorseRadish Peroxidase (HRP)- conjugated Goat anti-Rabbit Ig (Southern Biotech) was used as the secondary antibody. Membranes were then washed 5x with TBST. For HRP detection, membranes were developed with SuperSignal West Pico PLUS Chemiluminescent Substrate (Fisher Scientific), and chemiluminescent signal was detected with a ChemiDoc Imaging System (BioRad). For Europium detection, membranes were imaged using the time-resolved fluorescence ScanLater Western Blot protocol on the SpectraMax iD5 (Molecular Devices).

Indirect enzyme-linked immunosorbent assays

96-well high-binding polystyrene plates (Corning, 9018) were coated with 2 μ g/mL rRBD (Sino Biologicals, 40592-V08H) overnight at 4°C, with gentle shaking. The plates were then blocked with blocking solution (TBST +1% BSA) for 1 h at 37°C and then washed 5x with TBST. For antibody standards, monoclonal human anti-RBD mAb (Sino Biological) was added to wells at concentrations ranging from 50 to 0.8 μ g/mL. Purified antibodies from CCP samples were added to plates at total antibody concentrations ranging from 500 to 7.8 μ g/mL. Plates were incubated at 37°C for 1 h with gentle shaking and washed 5x with TBST. For detection, 50 μ L Goat α -Human IgG H + L-AP (Southern Biotech) was added at a concentration of 1 μ g/mL and the plates were again incubated at 37°C for 1 h and washed 5x with TBST. 50 μ L 1 mg/mL of *para*-nitrophenylphosphate (PNPP; Sigma) substrate was added to determine the concentration of antibody in each well and the absorbance at 405 nm was measured in each well with the EMax Plus Microplate reader (Molecular Devices). Absorbances from the CCP antibody were interpolated into the standard curve to determine the percentage of RBD-specific antibody in each CCP sample.

Virus inactivation procedure

Vero TMPRSS2 cells in flasks with 90–100% confluence were infected with the specific SARS-CoV-2 isolate at a multiplicity of infection (MOI) of 0.01, incubated for 3 days at 33°C, upon which virus supernatant was collected, centrifuged, and inactivated with the addition of 0.05% β -propiolactone and incubation at 4°C for 24 h followed by a 2 h 37°C incubation. The inactivated virus particles were purified by ultracentrifugation in a Beckman SW28TU rotor at 25,000 rpm for 1 h at 4°C with a 20% sucrose gradient and the virus pellet was resuspended in 1X PBS+. To confirm the virus had been successfully inactivated, a TCID₅₀ assay was performed.⁷² A bicinchoninic acid assay (BCA; Pierce) was used to estimate the relative viral protein concentration.

Plaque reduction neutralization test (PRNT) assay

The SARS-CoV-2 PRNT has been described previously.⁷³ Briefly, VeroE6-TMPRSS2 cells were seeded in a sterile 6-well plate and incubated at 37°C until 100% confluent. Heat-treated CCP3 convalescent plasma or purified IgG samples (stock = 17.1 mg/mL total IgG, 4.78 μ g/mL α -RBD IgG) were diluted to 1:20 using DMEM containing 2.5% FBS (Gibco, Thermo Fisher Scientific), 1 mM glutamine (Invitrogen, Thermo Fisher Scientific), 1 mM sodium pyruvate (Invitrogen, Thermo Fisher Scientific), 100 U/mL penicillin (Invitrogen, Thermo Fisher Scientific), and 100 μ g/mL streptomycin (Invitrogen, Thermo Fisher Scientific)⁴⁰ and serially diluted in 2-folds until 1:2560. Each dilution and a non-plasma control were incubated with 100 plaque-forming units (PFU) of a SARS-CoV-2 clade A.3 isolate. For each experiment, three sets of diluted samples were prepared. The first set of virus-plasma mixtures were incubated for 1 h at RT, the second set of samples were incubated for 6 h at 37°C, and the third set was incubated for 6 h at 4°C. After the incubation 250 μ L of each mixture was overlaid on VeroE6-TMPRSS2 monolayers in duplicate wells for 1 h at 37°C. Then the virus-plasma mixture was carefully aspirated and 2 mL of sterile 1% methylcellulose (a mixture of equal parts 2% methylcellulose (Sigma) and equal parts of 2X MEM (Gibco) supplemented with 1% Penicillin and Streptomycin, 1% GlutaMAX and 10% FBS) were overlaid into each well and incubated for 48 h at 37°C. The plates were then fixed with 4% formaldehyde overnight and stained with Naphthol Blue Black. IC₅₀ was calculated based on PFU counts using the inhibition dose-response, non-linear regression model using the GraphPad Prism 9 software.

QUANTIFICATION AND STATISTICAL ANALYSIS

Statistical analysis

Data were analyzed in Excel (Microsoft, Redmond, WA) and graphed in Prism 9.0 (Graphpad, San Diego, CA). For the two CCP cohorts, Spearman correlations of epitope cleavage observed by FRET for RBM1 or RBM2 and donor age or days since PCR positive diagnosis of COVID-19, anti-Spike antibody or nAb AUC were conducted. Missing data were excluded (available case method). Analysis was performed in R 4.2.1 (R Core Team, Vienna, Austria). Statistical significance for PRNT data was measured using the Mann Whitney matched rank test, using GraphPad Prism. Two-tailed p value <0.05 was considered statistically significant.